

Department of Physics and Astronomy
University of Heidelberg

Bachelor Thesis in Physics

submitted by

Tobias Denz

born in Friedberg (Hesse, Germany)

2013

Simple Phenomenological Models for Anisotropic Direct Photon Production in Heavy-Ion Collisions

This bachelor thesis has been carried out by Tobias Denz at the
Physikalisches Institut in Heidelberg
under the supervision of
Priv.-Doz. Dr. Klaus Reygers

Abstract

The LHC experiment ALICE focuses on investigating the quark gluon plasma by heavy-ion collisions. Recent ALICE measurements of Pb-Pb collisions at $\sqrt{s_{\text{NN}}} = 2.76$ TeV show a direct photon elliptic flow which is larger than it had been previously predicted to be by hydrodynamical calculations. This might be explained by a substantial direct photon production during the later stages of the collision system evolution where hadron flow is prevalent. To test this hypothesis, three simple phenomenological models have been developed in this thesis. They are fitted to experimental data from ALICE, PHENIX, and WA98 as well as compared to hydrodynamical calculations. The models describe the data mostly very well, yet exhibit a broad region of valid fit parameter combinations. Thus, a consistent description of direct photons and thermal charged pions stemming from a source with prevalent hadron flow can be achieved within these regions.

Zusammenfassung

Das Teilchenbeschleunigerexperiment ALICE hat das Ziel, das Quark-Gluon-Plasma mit Hilfe von Schwerionenkollisionen zu untersuchen. Kürzlich publizierte Messungen von Blei-Blei-Kollisionen bei $\sqrt{s_{\text{NN}}} = 2.76$ TeV am ALICE-Detektor zeigen einen elliptischen Fluss direkter Photonen, der weitaus größer ist, als bei herkömmlichen hydrodynamischen Modellrechnungen erwartet wird. Dies könnte dadurch erklärt werden, dass eine nicht vernachlässigbare Produktion direkter Photonen in einer späten Phase der Entwicklung des Kollisionssystems stattfindet, in der Hadronenfluss vorherrscht. In dieser Bachelorarbeit werden drei einfache phänomenologische Modelle entwickelt, um diese Hypothese zu überprüfen. Sie werden an Messdaten von ALICE, PHENIX und WA98 gefittet sowie mit hydrodynamischen Rechnungen verglichen. Die Modelle können die Daten gut beschreiben, zeigen jedoch einen großen Freiraum für die Fitparameter. Innerhalb dieser Freiräume gelingt eine konsistente Beschreibung von direkten Photonen und geladenen Pionen aus einer Quelle mit Hadronenfluss.

Contents

1	Introduction	1
2	Theory	4
2.1	Natural Units	4
2.2	Heavy-Ion Collisions	4
2.3	Evolution of an ideal QGP	5
2.4	Anisotropic Flow	6
2.5	Lorentz Transformations	7
3	Simple Collective Flow Models	8
3.1	Forward Emission Model	8
3.1.1	Assumptions of the Forward Emission Model	8
3.1.2	Mathematical Description of the Forward Emission Model	9
3.2	Isotropic Emission Model	10
3.2.1	Assumptions of the Isotropic Emission Model	10
3.2.2	Mathematical Description of the Isotropic Emission Model	11
3.3	Comparison of the Photon Models	12
3.4	Forward Emission Model for Massive Particles	13
4	Fits to Various Data Sets	15
4.1	Methodology	15
4.1.1	Implementation	15
4.1.2	Parameter Constraints	16
4.2	ALICE Direct Photon Data	16
4.2.1	pQCD Contribution	16
4.2.2	Forward Emission Model	18
4.2.3	Isotropic Emission Model	20
4.3	PHENIX Data	22
4.3.1	pQCD Contribution	22
4.3.2	Forward Emission Model	24
4.3.3	Isotropic Emission Model	24
4.4	WA98 Data	29
4.5	Theoretical Hydrodynamical Calculations	29
4.5.1	Forward Emission Model	30
4.5.2	Isotropic Emission Model	32
4.6	ALICE π^\pm Data	32

Contents

5 Outlook	37
5.1 Time Evolution Model	38
6 Conclusions	40
Bibliography	42
Acknowledgements	45
Erklärung/Declaration	47

1 Introduction

In the beginnings of the twentieth century, the developments of general relativity and quantum mechanics lead to ever improving theories to describe the fundamental laws of nature. New experiments and detectors were designed to test these theories. In particle physics this gave rise to the so-called Standard Model of particle physics, which has been very successful in describing and predicting effects of electromagnetic, weak and strong nuclear interactions, although it fell short of being a theory of everything [1].

In the early twenty-first century all but one particle predicted by the Standard Model, the Higgs boson, had been found. Thus, two of the main goals of the Large Hadron Collider (LHC), which was built by the European Organization for Nuclear Research (CERN) and first started up in 2008, were the experimental confirmation of the existence of the Higgs boson and the testing of theories going beyond the Standard Model [2, 3].

One of the four large detector experiments at the LHC is A Large Ion Collider Experiment (ALICE). It focuses mainly on heavy-ion collisions and aims to study the properties of the quark-gluon plasma (QGP) [4]. The quark-gluon plasma is a state of matter at very high temperature and/or pressure in which quarks and gluons are deconfined.

Some important measures in ultra-relativistic heavy-ion collisions are the initial temperature of the QGP and the elliptic flow of the system, which is quantified by the parameter v_2 . However, recent results [5] show a direct photon¹ elliptic flow (see figure 1.1) which is much larger than generally predicted by recent hydrodynamical descriptions. Because their yield is proportional to the square of the temperature, the direct photons are in those descriptions assumed to form mainly in the early hot phase of the QGP, which would make their spectrum a relatively good measure for its initial temperature.

A possible alternative that might explain the v_2 results is that the photons form to a significant extent during a later stage of the system. In the later stages the QGP evolves into a hadron gas (HG), and a strong collective flow is prevalent. Consequently, those

¹ The direct photons are photons emerging directly from particle collisions [6].

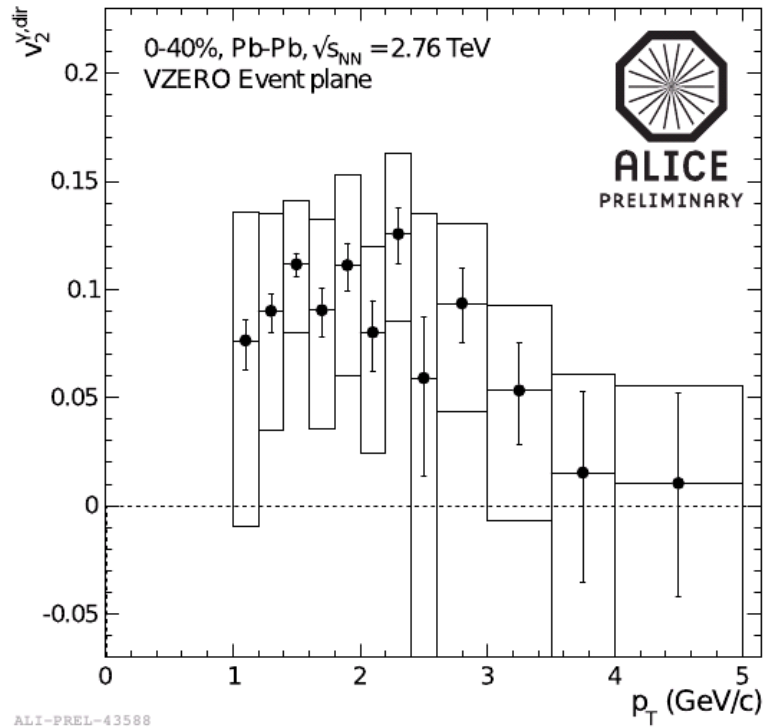


Figure 1.1: Recent ALICE measurements show a direct photon elliptic flow which is larger than had been predicted by theoretical calculations [5].

photons would undergo a blue- or redshift, and not be a direct measure for the initial temperature.

The main goal of this bachelor thesis is to use simulations based on simple phenomenological models to test this hypothesis. For this purpose two basic models were developed that describe and can fit a direct photon and v_2 spectrum simultaneously, as well as a similar model for thermal hadrons like charged pions. All three models were tested against several data sets.

To this end, the models have been implemented as functions in ROOT [7], a framework for large scale data handling and analysis, which is widely used in high energy particle physics and other fields. Then they were fitted to these data sets, again using ROOT.

In this way, it was possible to describe several of the direct photon measurements relatively well. On the other hand, the limitations of the models due to their simple nature became apparent. Ultimately, a comparison between the fits to the ALICE direct photon and charged pion data lead to the conclusion that a consistent description of photons and pions is possible. Therefore, a scenario where direct photons arise mainly

in a later phase of the QGP evolution respectively in the HG phase should not be ruled out on the basis of these models.

The thesis consists of five main parts following this introduction. First, Chapter 2 will give an overview over the basic theoretical background needed for the subject matter. Next, chapter 3 will introduce and describe the used models, while chapter 4 will deal with their fits to the data and present the respective results. Finally, possible next steps will be outlined, and the contents and results of the thesis will be summarised.

2 Theory

This chapter aims to give an overview over the most important and relevant theoretical background for this thesis. For a more in-depth discussion consult e.g. the books of Yagi, Hatsuda and Miake [8], Vogt [9], or Florkowski [10], which have also been used as resources for the information in this chapter.

2.1 Natural Units

Throughout this thesis natural units will be used, unless explicitly stated otherwise. Natural units in this context refer to the convention that the speed of light c , the reduced Planck constant \hbar , and the Boltzmann constant k_B [11] are all set to unity:

$$c = 299\,792\,458 \frac{\text{m}}{\text{s}} = 1, \quad \hbar = 1 \simeq 6.5821 \cdot 10^{-16} \text{ eV s}, \quad k_B = 1 \simeq 8.6173 \cdot 10^{-5} \frac{\text{eV}}{\text{K}}. \quad (2.1)$$

This conveniently allows to express all other units relevant for this thesis in femtometre (fm), which is the typical length scale of a nucleus, or giga-electronvolt¹ (GeV):

$$1 \text{ fm} \simeq 3.3346 \cdot 10^{-24} \text{ s} \simeq 5.0677 \frac{1}{\text{GeV}} \quad (2.2)$$

$$1 \text{ GeV} \simeq 1.1605 \cdot 10^{13} \text{ K} \simeq 1.7827 \cdot 10^{-27} \text{ kg} \simeq 5.0677 \frac{1}{\text{fm}} \quad (2.3)$$

2.2 Heavy-Ion Collisions

In particle accelerators like the Super Proton Synchrotron (SPS) and the LHC at CERN, or the Relativistic Heavy Ion Collider (RHIC) at the Brookhaven National Laboratory (BNL), heavy ions are accelerated to ultra-relativistic speeds.

¹ An electronvolt is the change in kinetic energy of an electron accelerated by an electric potential difference of one volt (V). In SI units $1 \text{ eV} \simeq 1.6022 \cdot 10^{-19} \text{ J}$ [11].

At those speeds the ions are length-contracted into very flat discs and, at center-of-mass (CMS) energies of more than $\sqrt{s_{\text{NN}}} \approx 100 \text{ GeV}$, their valence quarks pass through each other, i.e., they are said to be transparent [8]. In the space between them, hot matter with a high energy density and low baryon density is generated. At lower center-of-mass energies the nuclei do not pass through each other, but instead could form a phase with high temperature and baryon density upon collision.

Both cases could lead to the formation of a quark-gluon plasma (QGP) [8], which is a state of matter predicted by quantum chromodynamics (QCD) at very high temperatures above the pseudo-critical temperature T_c and/or high baryon densities above about five times the normal nuclear matter density [12]. Its constituents, namely those very quarks and gluons, are no longer confined in baryons and mesons and form an almost ideal gas. The QGP has with high probability indeed been observed at the aforementioned accelerators and high beam energies [13, 14].

2.3 Evolution of an ideal QGP

The QGP develops after a thermalisation phase at a characteristic eigentime $\tau_0 \lesssim 1 \text{ fm} \simeq 3.335 \cdot 10^{-24} \text{ s}$ and is then in local thermal equilibrium. Next, it starts to expand at a very fast rate, meanwhile cooling down accordingly [8].

Once the QGP has expanded and cooled until it reaches a temperature T_c of about 150 MeV to 160 MeV [15], a crossover transition to a hadron gas (HG) is expected to occur [16]. Afterwards the system continues to cool and expand as a HG until it reaches kinetic freeze-out at around the temperature $T_{\text{fo}} \approx 100 \text{ MeV}$ for central collisions [17], where elastic scattering breaks down. Then the mean free path of the hadrons becomes larger than the system itself, which means that the system can no longer be described hydrodynamically [9]. There is also the chemical freeze-out, which happens when inelastic processes cease and is believed to take place at about and slightly below T_c .

Meanwhile collisions, annihilation processes and particle decays lead to the production of photons. Photons stemming from particle decays are called decay photons, which make up the so-called inclusive photons together with the direct photons. The direct photons in turn consist of the perturbative QCD (pQCD) photons, the thermal photons, which stem from the thermal movement of the quarks, gluons, and hadrons, as well as pre-equilibrium photons, which are the radiation from a medium that has not yet reached thermal equilibrium [6].

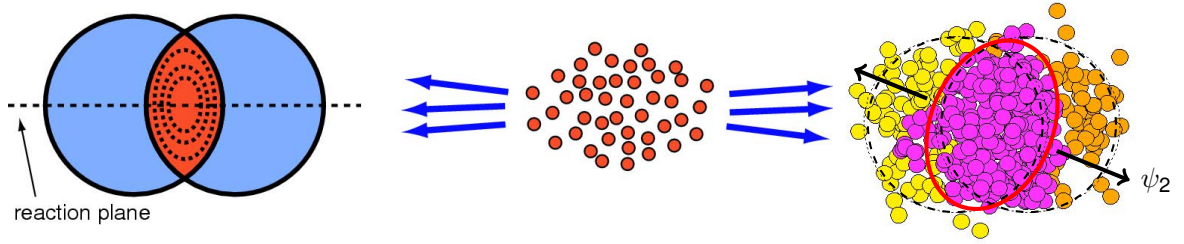


Figure 2.1: Non-central collisions (left) give rise to an anisotropic flow (middle) [18]. Fluctuations (right [19]) add to this effect.

2.4 Anisotropic Flow

The collisions of the length-contracted ions at ultra-relativistic speeds are usually not completely central. The 2-D vector pointing from the center of one of the colliding nuclei to the other in the plane perpendicular to the beam axis is called the impact vector and spans the reaction plane with the beam axis [10]. The length of the impact vector is called the impact parameter and directly related to the centrality².

The non-central collisions and the fluctuations of the nucleons' positions in the nuclei give rise to anisotropies in the collision zone (see fig. 2.1). Consequently, a pressure gradient builds up which results in a collective flow that is stronger in the direction of the reaction plane. Thus, the emerging invariant yield³ can be expanded as a Fourier series [10]:

$$E \frac{d^3N}{dp^3} = \frac{1}{2\pi} \frac{d^2N}{p_T dp_T dy} \left(1 + 2 \sum_{n=1}^{\infty} v_n \cos(n(\varphi - \psi_n)) \right), \quad (2.4)$$

where E is the energy, N the particle number, p the momentum and p_T the transverse momentum, i.e. the momentum component transverse to the beam axis, y the rapidity, and the ψ_n are the angles of the planes the corresponding harmonic of the anisotropic flow refers to. In this thesis the second parameter v_2 , also called the elliptic flow parameter, will feature most prominently.

² The experimental centrality is a measure defined as the fraction of events that has the highest multiplicity, i.e. number of produced particles per given hadron-hadron collision [9].

³ Sometimes the term 'photon spectrum' will be used to refer to the photon invariant yield throughout this thesis.

2.5 Lorentz Transformations

In special relativity, a Lorentz transformation is a linear transformation from one frame into another. Lorentz transformations without rotation are also called Lorentz boosts.

An easy way to obtain the energy E' of an object with the four-momentum⁴ $\mathbf{p}^\mu = (E, \vec{p})$ in one frame boosted into a different frame with the same origin that is moving with the relative three-velocity $\vec{\beta}$ is to contract \mathbf{p} with the corresponding four-velocity $\mathbf{U}^\mu = \gamma \cdot (1, \vec{\beta})$, where $\gamma = (1 - \beta^2)^{-\frac{1}{2}}$ and $\beta = |\vec{\beta}|$. Then the energy in the boosted frame is

$$E' = p^\mu U_\mu = \gamma \cdot (E - \vec{p} \cdot \vec{\beta}) = \gamma \cdot (E - p\beta \cos(\theta)) = \gamma E \cdot \left(1 - \frac{p}{E} \beta \cos(\theta)\right), \quad (2.5)$$

where $\theta = \angle(\vec{p}, \vec{\beta})$ and $p = |\vec{p}|$.

For a photon with $\mathbf{p}^\mu = (\omega, \vec{k})$, where $|\vec{k}| = \omega$, this becomes

$$E' = \omega' = \gamma\omega \cdot (1 - \beta \cos(\theta)) \quad \text{and} \quad (2.6)$$

$$E' = \omega' = \gamma\omega \cdot (1 - \beta) = \omega \cdot \sqrt{\frac{1 - \beta}{1 + \beta}} \quad \text{in the case } \theta = 0. \quad (2.7)$$

⁴Regarding the notation of vectors, three-vectors will generally be denoted by arrows, e.g. \vec{p} , while four-vectors are represented as bold symbols, e.g. \mathbf{p} . Upper and lower indices on four-vectors distinguish between contravariant and covariant vectors, respectively. The Einstein summation convention is used where appropriate.

3 Simple Collective Flow Models

During the course of this bachelor thesis three simple, static models describing direct photon invariant yields and the direct photon elliptic flow v_2^{dir} , as well as the thermal invariant yield and the thermal elliptic flow v_2^{th} of hadrons, in each case originating from a single fluid cell with a collective flow, have been developed. All three models were designed to be used to fit to an invariant yield spectrum and a v_2 spectrum simultaneously.

3.1 Forward Emission Model

The first and more basic of the two models describing direct photons will in the following be called the forward emission model (FEM). The FEM was designed to provide a very simple yet sufficiently accurate description of both data sets.

3.1.1 Assumptions of the Forward Emission Model

In the FEM it is assumed that the situation is static, i.e. the time evolution of the system is neglected. This is equivalent to the case where the photon production is dominated by a single stage of the evolving system with a certain temperature T and a certain flow velocity profile. The photon sources, namely the quarks and gluons respectively hadrons, should be in thermal equilibrium, that is, the photon spectrum is taken to follow a simple Boltzmann distribution in the transverse momentum p_T in the sources' rest frame. It is also initially assumed that the photon source is a fireball consisting of one fluid cell only. The fluid in this cell is subject to a collective flow whose strength is modulated with its direction relative to the collision plane. In addition, the photons in the FEM get emitted and boosted only in the direction of the collective flow.

This especially means that this model allows only for blueshifted photons which are boosted with exactly the speed of the collective flow. Then the thermal photon and

v_2 spectrum are averaged over an angle of 2π in the laboratory system. Finally, the contribution of the pQCD photons is added, or, respectively, factored in to get a final result that is comparable to the data.

3.1.2 Mathematical Description of the Forward Emission Model

Due to the thermal equilibrium, the photons are following a Boltzmann distribution in the fluid cell's rest frame: $\left(E \frac{d^3 N_\gamma}{dp^3}\right)^{\text{th}} \propto \exp\left(\frac{p_T}{T}\right)$, where $p_T = |\vec{p}_T|$, $\vec{p}_T \perp \vec{e}_z$ is the momentum component transverse to the beam axis \vec{e}_z and T the temperature of the QGP.

The collective flow is modulated in the transverse rapidity

$$\rho(\varphi_\beta) = \rho_0 \cdot (1 + 2a_2 \cos(2\varphi_\beta)), \quad (3.1)$$

where φ_β is the laboratory angle with respect to the reaction plane, ρ_0 the mean transverse rapidity and a_2 a modulation strength parameter. The velocity β can then simply be calculated as $\beta(\varphi_\beta) = \tanh(\rho(\varphi_\beta))$. This leads to a Lorentz boosted transverse momentum in the laboratory frame as shown in equation (2.7):

$$p_T \rightarrow p_T \cdot \sqrt{\frac{1 - \beta(\varphi_\beta)}{1 + \beta(\varphi_\beta)}}. \quad (3.2)$$

The thermal photon invariant yield is then described as the normalised average over the angle φ_β :

$$\left(E \frac{d^3 N_\gamma}{dp^3}\right)^{\text{th}}(p_T) = \int_0^{2\pi} \frac{d\varphi_\beta}{2\pi} A \cdot \exp\left(-\frac{p_T}{T} \cdot \sqrt{\frac{1 - \beta(\varphi_\beta)}{1 + \beta(\varphi_\beta)}}\right), \quad (3.3)$$

where A is a scaling parameter. From there the thermal photon v_2^{th} can be calculated as

$$v_2^{\text{th}}(p_T) = \langle \cos(2(\varphi - \psi_2)) \rangle(p_T) = \frac{\int_0^{2\pi} d\varphi_\beta \cos(2\varphi_\beta) \cdot \frac{d}{d\varphi_\beta} \left(E \frac{d^3 N_\gamma}{dp^3}(p_T)\right)}{E \frac{d^3 N_\gamma}{dp^3}(p_T)}. \quad (3.4)$$

3 Simple Collective Flow Models

For the direct photon yield and v_2^{dir} the contribution of pQCD photons have to be added, so that

$$\left(E \frac{d^3 N_\gamma}{dp^3}\right)^{\text{dir}} = \left(E \frac{d^3 N_\gamma}{dp^3}\right)^{\text{th}} + \left(E \frac{d^3 N_\gamma}{dp^3}\right)^{\text{pQCD}} \quad \text{and} \quad (3.5)$$

$$v_2^{\text{dir}} = \frac{N_\gamma^{\text{th}}}{N_\gamma^{\text{dir}}} \cdot v_2^{\text{th}} + \frac{N_\gamma^{\text{pQCD}}}{N_\gamma^{\text{dir}}} \cdot \underbrace{v_2^{\text{pQCD}}}_{=0} = \frac{N_\gamma^{\text{th}}}{N_\gamma^{\text{dir}}} \cdot v_2^{\text{th}}, \quad (3.6)$$

where the elliptic flow parameter of the pQCD photons v_2^{pQCD} is usually assumed to be zero. The factor $N_\gamma^{\text{th}}/N_\gamma^{\text{dir}}$ can be parametrised as follows:

$$\left. \frac{N_\gamma^{\text{th}}}{N_\gamma^{\text{dir}}} \right|_{p_T} = \left. \frac{N_\gamma^{\text{th}}}{N_\gamma^{\text{th}} + N_\gamma^{\text{pQCD}}} \right|_{p_T} \simeq \frac{1 + e^{-\frac{P_0}{P_1}}}{1 + e^{-\frac{p_T - P_0}{P_1}}}, \quad (3.7)$$

where P_0 and P_1 are fit parameters.

This factor could also be used to scale the thermal to the direct invariant yield, i.e.

$$\left(E \frac{d^3 N_\gamma}{dp^3}\right)^{\text{dir}} = \frac{N_\gamma^{\text{dir}}}{N_\gamma^{\text{th}}} \cdot \left(E \frac{d^3 N_\gamma}{dp^3}\right)^{\text{th}}. \quad (3.8)$$

However, since $N_\gamma^{\text{th}}/N_\gamma^{\text{dir}}$ gets very small for high p_T values, this calculation is very error-prone in those regions. Therefore the direct adding of the pQCD contribution has been preferred.

3.2 Isotropic Emission Model

The second model is called the isotropic emission model (IEM) and slightly more complex. It was designed as an extension of the FEM in order to provide a more accurate description of the data.

3.2.1 Assumptions of the Isotropic Emission Model

The basic assumptions of the IEM are mainly the same as in the FEM. However, the way the photons are emitted is fundamentally different. While the assumption of the FEM that photons get boosted only in the direction of the collective flow allows for a

simple calculation and might be regarded as sufficient in order to describe a blueshift, it is strictly speaking wrong. The reason for this is that the photons should get created isotropically in the rest frame fluid cell. The collective flow does then only lead to a shift of the frequency of the photon via a Lorentz boost, but not to a change in direction, since the speed of light is constant in all reference frames. It should also be noted that the mean free path of the photons is much larger than the size of the fireball, so that they are able to traverse the QGP unobstructed.

Therefore the IEM assumes that the photons get emitted and boosted isotropically. Thus it allows for photons that are redshifted as well as for blueshifted photons, where the extent of the red- or blueshift depends on the angle between the directions of the photon and the collective flow. The spectra are then averaged over this angle as well as the angle between the direction of the collective flow and the collision plane.

3.2.2 Mathematical Description of the Isotropic Emission Model

Since the IEM is in large part very similar to the FEM, the mathematical description is also mostly identical. Thus the collective flow modulation is exactly as described in equation (3.1). However, comparable to equation (2.6), the Lorentz boost now also depends on the angle between the collision plane and the photon direction φ_p , because the photons are emitted isotropically:

$$p_T \rightarrow p_T \cdot \frac{1 - \cos(\varphi_\beta - \varphi_p) \cdot \beta(\varphi_\beta)}{\sqrt{1 - \beta^2(\varphi_\beta)}}. \quad (3.9)$$

Consequently, the thermal photon spectrum is the normalised average over the two angles φ_β and φ_p :

$$\left(E \frac{d^3 N_\gamma}{dp^3} \right)^{\text{th}}(p_T) = \int_0^{2\pi} \frac{d\varphi_\beta}{2\pi} \int_0^{2\pi} \frac{d\varphi_p}{2\pi} A \cdot \exp \left(-\frac{p_T}{T} \cdot \frac{1 - \cos(\varphi_\beta - \varphi_p) \cdot \beta(\varphi_\beta)}{\sqrt{1 - \beta^2(\varphi_\beta)}} \right). \quad (3.10)$$

The direct photon invariant yield, v_2^{th} , and v_2^{dir} are then again calculated exactly as in equations (3.4) to (3.8).

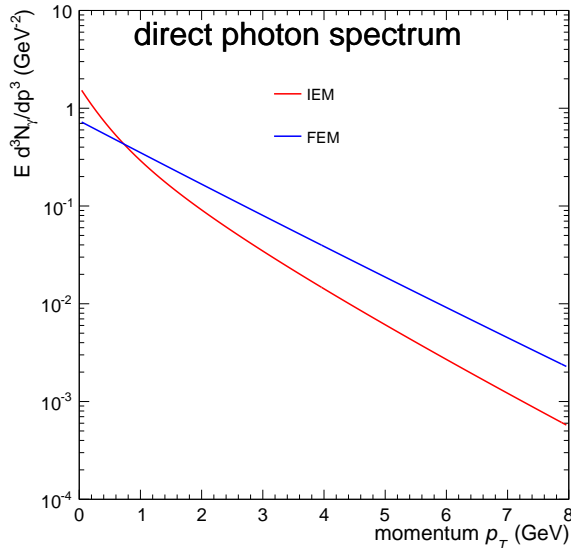


Figure 3.1: The redshift contribution in the IEM manifests itself in a steeper slope for low transverse momenta.

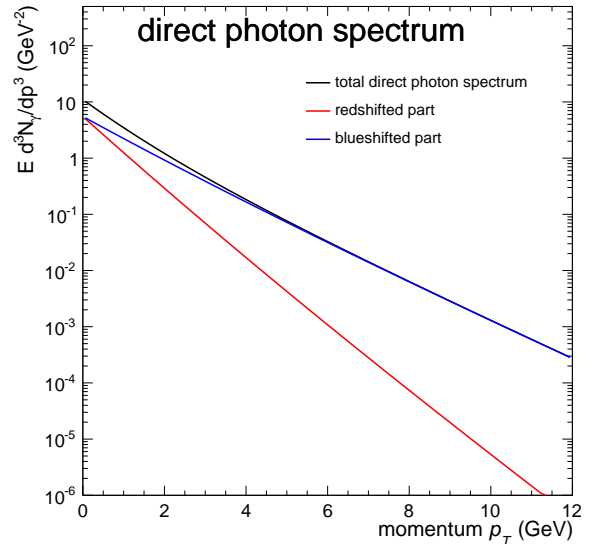


Figure 3.2: The redshifted component in the IEM drops considerably faster than the blueshifted one.

3.3 Comparison of the Photon Models

Despite their similarities the two photon models have one key difference, which is that the FEM only considers photons emitted in the direction of the collective flow. That means that it is much simpler and does simply ignore a big part of the actual physics. On the other hand, its very simplicity makes calculations much faster than in the IEM, which involves two integrations during every evaluation of the direct photon spectrum. This can make a big difference in the total time needed for a fit with many iterations and several function calls for different values of p_T each time.

Phenomenologically, the absence of a redshifted component in the FEM should also show in the spectrum, especially at low p_T , since a redshift leads to a steeper slope of the spectrum. As one can see in figure 3.1, where the spectra of the two models have been plotted with identical parameters apart from the absolute normalisation, this is indeed the case. While the spectrum of the FEM is linear in logarithmic representation, the spectrum of the IEM has an additional rise towards low p_T . One can see that this is indeed due to the redshifted component if one looks at the composition of the spectrum as in figure 3.2. For high transverse momenta the contribution of the redshift is increasingly negligible and the spectra qualitatively identical.

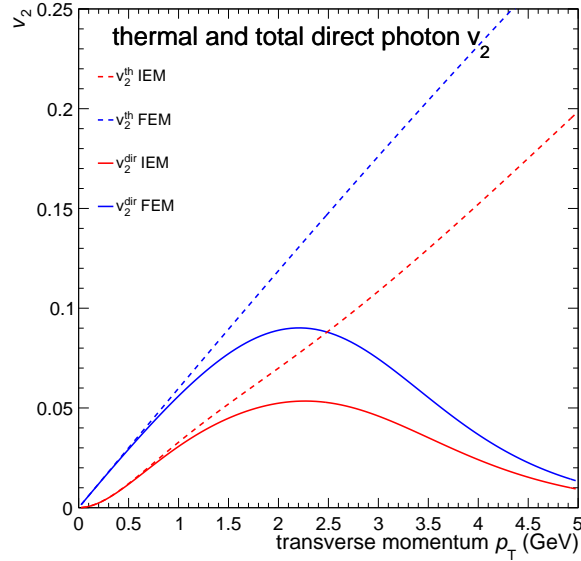


Figure 3.3: Comparison of the v_2 spectra of the two collective flow models. The dotted lines represent the thermal v_2^{th} , the continuous lines the direct v_2^{dir} . The FEM spectra are depicted in blue, the spectra of the IEM in red.

The comparison of the v_2 spectra (see figure 3.3) also shows a notable difference at low p_T , where the v_2 spectra of the IEM increases more slowly, until it reaches the same slope as in the FEM. On this account the v_2 IEM spectra are overall much flatter.

This can also be taken as an a posteriori legitimation of the FEM, since the results are still relatively similar, while the reduction of computation time is comparatively large. However, it should not be forgotten that there are differences in the models and that the same parameters will describe different spectra or the same spectra would correspond to different parameters, especially for low p_T data points in the direct photon spectra and for the v_2 data.

3.4 Forward Emission Model for Massive Particles

Massive particles like pions, which will be used as a comparison for the photon fits later on, have a much smaller mean free path than photons and can therefore not cross the fireball unaffected. Thus one can simplifyingly apply the FEM to describe the emerging spectrum.

However, since their rest mass m is non-zero, the equations need to be modified accordingly. First of all, the spectrum in the rest frame is taken to follow a Boltzmann

3 Simple Collective Flow Models

distribution in the transverse mass $m_T = \sqrt{m^2 + p_T^2}$ instead of the transverse momentum p_T . Furthermore, the rest mass gives rise to an additional factor $\sqrt{1 - (m/m_T)^2}$ in the Lorentz boost:

$$p_T \rightarrow p_T \frac{1 - \sqrt{1 - \left(\frac{m}{m_T}\right)^2} \cdot \beta(\varphi_\beta)}{\sqrt{1 - \beta^2(\varphi_\beta)}}. \quad (3.11)$$

The thermal spectrum is then described by

$$\left(E \frac{d^3 N_{\text{hadron}}}{dp^3}\right)^{\text{th}}(p_T) = \int_0^{2\pi} \frac{d\varphi_\beta}{2\pi} A \cdot \exp\left(-\frac{p_T}{T} \cdot \frac{1 - \sqrt{1 - \left(\frac{m}{m_T}\right)^2} \cdot \beta(\varphi_\beta)}{\sqrt{1 - \beta^2(\varphi_\beta)}}\right). \quad (3.12)$$

From there, the thermal elliptic flow parameter v_2^{th} is computed as in equation (3.4).¹

¹ The respective direct quantities are not calculated, because the ratio of thermal to direct particles is for experimental reasons for hadrons harder to determine than for photons. This is due to the fact that hadrons like pions get modified by the medium after their formation, while photons leave it mostly unmodified thanks to their longer mean free path.

4 Fits to Various Data Sets

The simple and static collective flow models were fitted to various data sets that usually consist of a direct photon invariant yield spectrum and an associated v_2^{dir} spectrum. This data sets stem from measurements at ALICE, PHENIX, and WA98¹. The collective flow photon models were also compared to hydrodynamical calculations by Holopainen et al.

4.1 Methodology

4.1.1 Implementation

All the different data sets in this chapter were fitted by means of methods provided by the ROOT software. In particular, the ROOT implementation of the MINUIT [20] minimisation program was used, mainly with the MIGRAD algorithm.

The fits were accomplished by minimising the χ^2 -function

$$\chi^2 = \frac{N_{\text{dps}} \cdot \chi_{\text{dps}}^2 + N_{v_2} \cdot \chi_{v_2}^2}{N_{\text{dps}} + N_{v_2}}, \quad \text{where} \quad (4.1)$$

$$\chi_{\text{dps}}^2 = \sum_{i=0}^{N_{\text{dps}}-1} \left(\frac{\left(E \frac{d^3 n_\gamma}{dp_T^3} \right)^{\text{exp}} - \left(E \frac{d^3 n_\gamma}{dp_T^3} \right)^{\text{theo}}}{\Delta \left(E \frac{d^3 n_\gamma}{dp_T^3} \right)^{\text{exp}}} \Bigg|_{(p_T, i)} \right)^2 \quad \text{and}$$

$$\chi_{v_2}^2 = \sum_{i=0}^{N_{v_2}-1} \left(\frac{v_2^{\text{dir,exp}} - v_2^{\text{dir,theo}}}{\Delta v_2^{\text{dir,exp}}} \Bigg|_{(p_T, i)} \right)^2,$$

for both spectra simultaneously². N_{dps} and N_{v_2} are the numbers of data points³ in the direct photon and v_2 spectrum, respectively.

¹ WA98 is the name of an experiment that took place at the CERN SPS.

² Another possibility would have been to add χ_{dps}^2 and $\chi_{v_2}^2$ directly, i.e. $\chi^2 = \chi_{\text{dps}}^2 + \chi_{v_2}^2$.

³ The values of the data points are referred to by 'exp' and the values of the model calculations by 'theo', even if the data points stem from other theoretical calculations.

4.1.2 Parameter Constraints

For all the following fits with either of the simple collective flow model, unless stated otherwise, the parameters have been constrained, based on basic physical considerations. The normalisation factor A was taken to be positive, i.e. in practice $10^{-3} \leq A \leq 10^5$. The temperature T should also be positive and was chosen as $0.01 \text{ GeV} \leq T \leq 0.5 \text{ GeV}$, since higher temperatures for the QGP are unlikely. For the mean rapidity $0 \leq \rho_0 \leq 1.2$ was chosen, which corresponds to the velocity range $0 \leq \beta \lesssim 0.8337$, because it should also be positive and higher rapidities are unlikely, as blast-wave fits result in velocities of $\langle \beta_T \rangle = 0.65$ for ALICE [21]. Since the rapidity should always stay positive, $0 \leq a_2 \leq 0.5$ was assumed for its modulation parameter a_2 .

4.2 ALICE Direct Photon Data

The ALICE direct photon data [22, 5] used in this thesis stem from central Pb-Pb collisions with 0–40% centrality and a centre of mass energy of $\sqrt{s_{\text{NN}}} = 2.76 \text{ TeV}$.

4.2.1 pQCD Contribution

In order to describe the direct photon invariant yield of the ALICE data, the contribution of the pQCD photons has to be added as in equation (3.5). The respective values of the pQCD photon contribution for $p_T \geq 2 \text{ GeV}$ have been calculated and provided by Werner Vogelsang [23].

The calculated values can be phenomenologically and reasonably described by a Hagedorn function

$$h(p_T) = h_0 \cdot \left(1 + \frac{p_T}{p_0} \right)^{-n}, \quad (4.2)$$

where h_0 , p_0 and n are fit parameters. This function describes the calculation very well up to the end of the chosen fit range at $p_T = 15 \text{ GeV}$, which lies well above the highest experimental data values used, as can be seen in figure 4.1. The fit results $h_0 = 3.873 \cdot 10^9 \text{ pb}$, $p_0 = 0.5107 \text{ GeV}$, and $n = 5.326$ have in the following been used to describe the pQCD contribution to the invariant yield. For this purpose, h_0 had to be scaled to the centrality class of the ALICE data by the corresponding factor $N_{\text{coll}}^{0-40\% \text{ cent.}} = 826.46$, which is the number of inelastic nucleon-nucleon collisions. Since

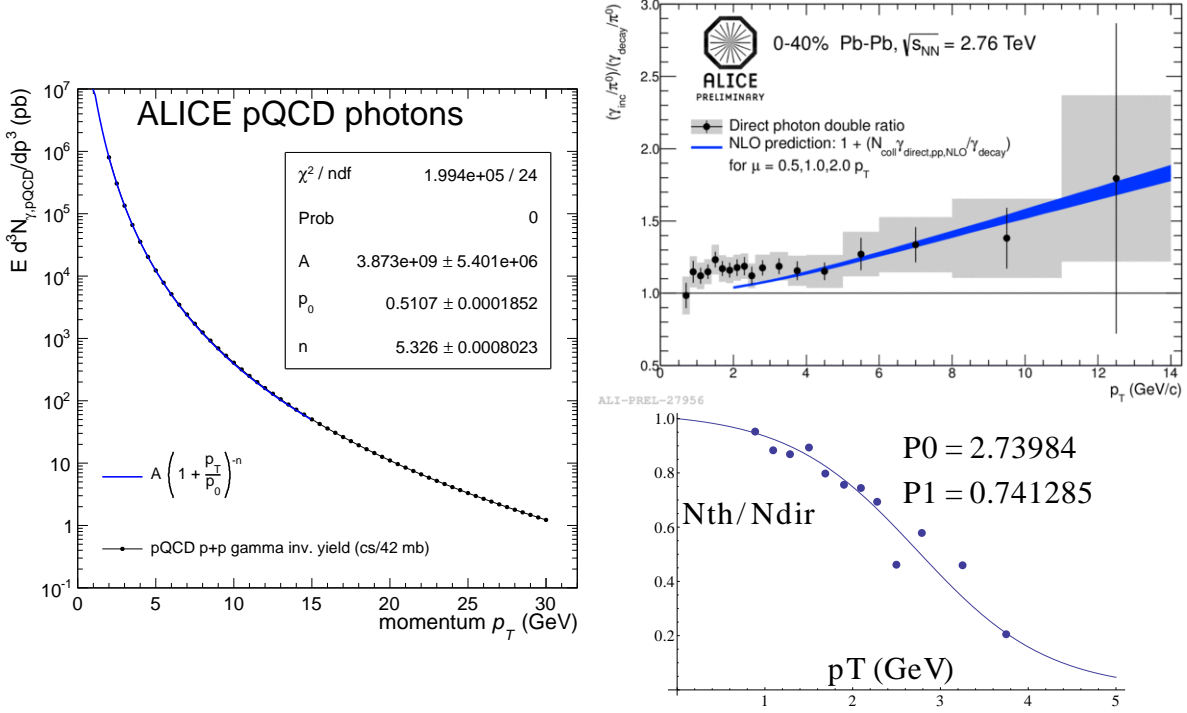


Figure 4.1: The ALICE pQCD photon calculation can be described very well by a Hagedorn function (left), which was consequently used to add the pQCD contribution to the invariant yield. For v_2^{dir} , the factors $N_{\gamma}^{\text{th}}/N_{\gamma}^{\text{dir}}$ were computed from the direct photon double ratio and corresponding pQCD calculation (top right [22]), and then fitted with Mathematica (bottom right).

the pQCD values were given as a cross section in pb, they had also to be converted to the invariant yield, which was given in GeV^{-2} .

For the calculation of v_2^{dir} , the factor $N_{\gamma}^{\text{th}}/N_{\gamma}^{\text{dir}}$ as a function of p_T still needed to be determined. For that purpose, the values have been calculated from the direct photon double ratio $N_{\gamma}^{\text{inc}}/N_{\gamma}^{\text{dec}}$ of the same measurement and the corresponding pQCD calculation $1 + N_{\gamma}^{\text{pQCD}}/N_{\gamma}^{\text{dec}}$, and then fitted with Mathematica (see figure 4.1) as follows:

$$\left. \frac{N_{\gamma}^{\text{th}}}{N_{\gamma}^{\text{dir}}} \right|_{p_T} = 1 - \left. \frac{N_{\gamma}^{\text{pQCD}}/N_{\gamma}^{\text{dec}}}{N_{\gamma}^{\text{inc}}/N_{\gamma}^{\text{dec}} - 1} \right|_{p_T} \simeq \frac{1 + e^{-\frac{P_0}{P_1}}}{1 + e^{-\frac{p_T - P_0}{P_1}}}. \quad (4.3)$$

The fit provided the results $P_0 = 2.740$ GeV and $P_1 = 0.7413$ GeV, which have been used below.

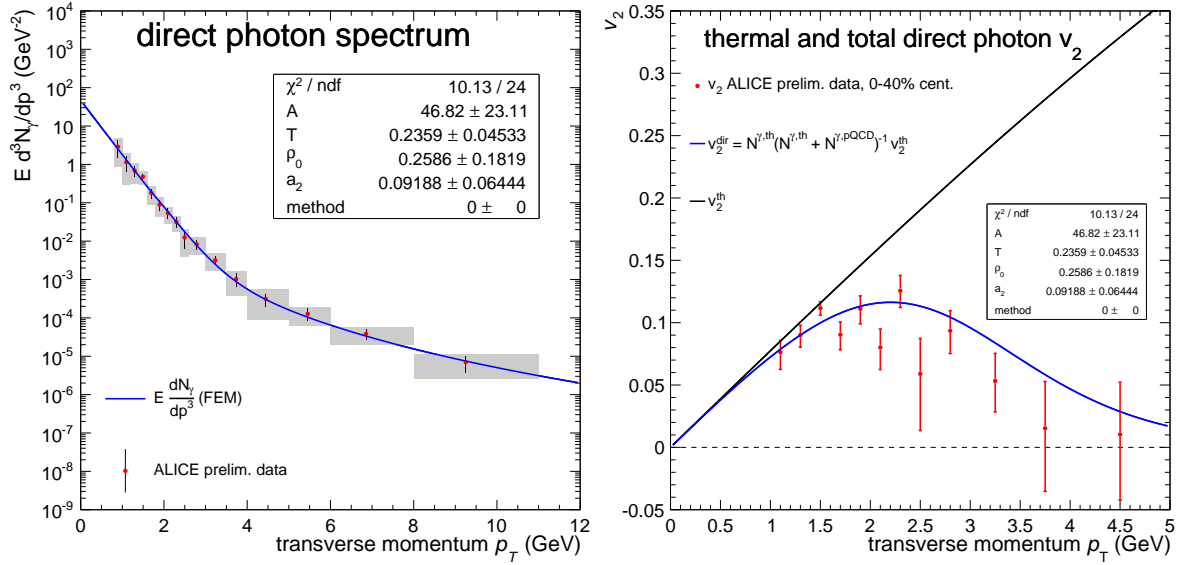


Figure 4.2: The ALICE direct photon invariant yield (left) and elliptic flow parameter v_2^{dir} (right) are described relatively well by the FEM.

4.2.2 Forward Emission Model

As can be seen in figure 4.2, the ALICE data are in general fitted relatively well by the FEM. The fit describes all the data points of the direct photon invariant yield within their error margins, although for higher p_T this is mainly due to the addition of the pQCD photon contribution.

The v_2^{dir} data are not described as good by the FEM. However, the data points themselves fluctuate much more here. Considering this, the description of the data at least up to about 2.3 GeV to 3 GeV seems to be reasonably good. On the other hand, all data points above 2.5 GeV lie systematically slightly below the fit, which suggests that the FEM is predicting too high v_2^{dir} values in this higher p_T range. Another factor is that the systematic errors of the v_2^{dir} measurement (cf. figure 1.1) have not been taken into account, since they are partly correlated, which makes a direct treatment difficult. Otherwise the fit would lie within the systematic error margins of almost all of the points.

Despite the reasonably good fit quality, it became apparent that the fit results differed depending on the initial parameters, indicating several possible fit parameter combinations. In order to test how the fit quality depended on the parameters, two different strategies were devised: The first strategy involves fixing the temperature T and fitting the remaining parameters A , ρ_0 and a_2 to the data for different values of T . For the sec-

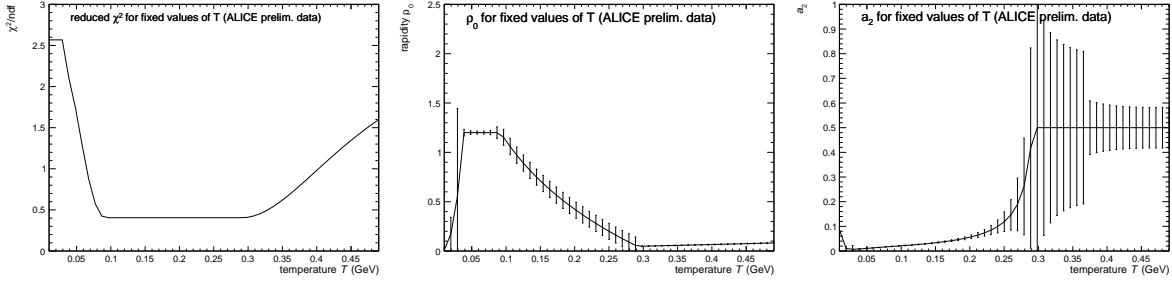


Figure 4.3: The χ^2 -values (left) for FEM fits with fixed temperature values and the corresponding results for ρ_0 (middle) and a_2 (right) show that there is a broad temperature region in which optimal fits are possible.

ond strategy the four parameters were passed through in a grid within given boundaries and the corresponding χ^2 value calculated for all respective parameter combinations. While the first strategy can only provide the best parameter combination and fit quality for each fixed value of T , the second strategy is potentially more time-consuming, since a large number of values has to be calculated to get a detailed overview.

If one now examines the parameter freedom for the ALICE data FEM fits by calculating the fit qualities for various fixed values of T between 0 GeV and 0.5 GeV (see figure 4.3), one can see that, indeed, in the temperature region $0.1 \text{ GeV} \lesssim T \lesssim 0.3 \text{ GeV}$ all fits seem to have equal probability. It is also noticeable that, in the temperature region of minimal χ^2 , ρ_0 drops from 1.1 to its minimal value of about 0.05, while a_2 rises from 0.02 to its parameter limit of 0.5.

Thus, one perceives that good fits with a low temperatures also have higher rapidities and lower a_2 values, while those with higher temperatures have low rapidities and higher a_2 values. The explanation for this relation between T and ρ_0 is that the temperature and the boostfactor together have to describe the slope of the thermal invariant yield. a_2 has then still to describe the elliptic flow.

The parameter A has usually not been regarded while examining the parameter freedom, because it did not change much with different start values. Moreover, A is simply a normalisation parameter for the invariant yield and as such less interesting than T , ρ_0 , or a_2 for the subject matter.

If one then looks at the parameter freedom by calculating the χ^2 values for the different parameter combinations and plotting the minimal values for combinations of two parameters (see figure 4.4), one notices that this seems to correspond to a broad valley in the ρ_0 - T -plane that is lengthwise divided by a small ridge and crossed by a

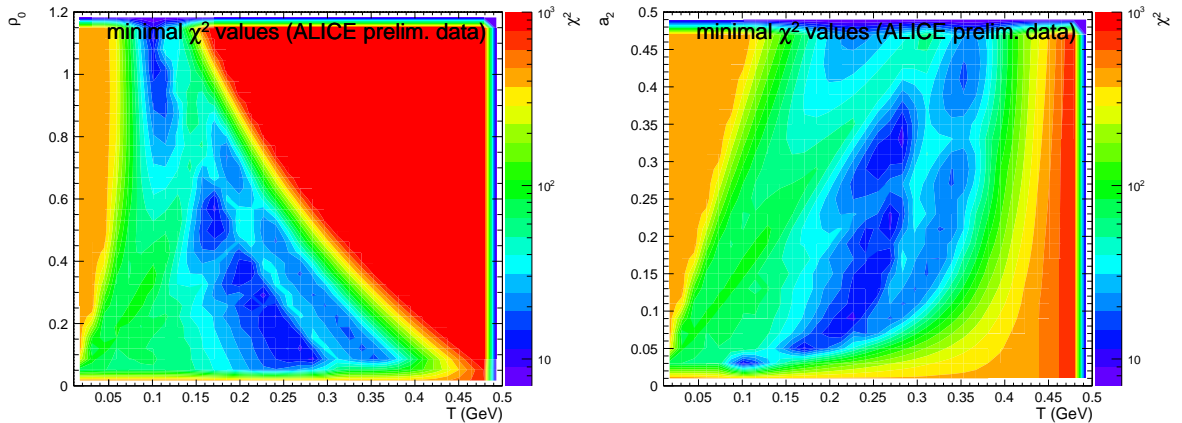


Figure 4.4: Minimal χ^2 values for parameter combinations of ρ_0 and T (left) as well as a_2 and T (right) illustrate the parameter freedom in the FEM.

bigger one between $T \approx 0.1$ GeV and $T \approx 0.15$ GeV, as well as several smaller ones. In the a_2 - T -plane, there is also a broad valley of low χ^2 values divided by a ridge at about $T \approx 0.3$ GeV. These good fit regions cover all rapidities above roughly $\rho_0 \approx 0.075$ up to $\rho_0 = 1.2$ and all a_2 values above about 0.03 up to 0.5 for 0.09 GeV $\lesssim T \lesssim 0.37$ GeV.

So, in conclusion, although the FEM can fit the ALICE data quite well, it is apparently not able to conclusively constrain the parameters to a single small area.

4.2.3 Isotropic Emission Model

While the FEM was already providing reasonable fits of the ALICE data, it is still of interest to see how the more complex IEM holds up in comparison. On the whole, the fits (see figure 4.5) describe the data about as well as the FEM. Only for higher p_T values are the systematic deviations in the v_2^{dir} spectrum slightly larger.

The parameters are also still relatively free, as can be seen when fitting the data for fixed temperature values (see figure 4.6). Although the χ^2 values follow a similar trend as in the FEM, they are no longer constant in the region of best fits between about $T \simeq 0.08$ GeV and $T \simeq 0.25$ GeV, and have a minimum at $T \approx 0.1$ GeV. The corresponding ρ_0 and a_2 values now look a bit different than in the FEM. In particular, the rapidity now drops from its limit $\rho_0 = 1.2$ at $T \approx 0.1$ GeV to a minimum slightly below $\rho_0 = 0.3$ at $T \approx 0.35$ GeV. Meanwhile a_2 increases from about 0.03 at $T = 0.1$ GeV to a maximum of 0.4 at $T \approx 0.375$ GeV.

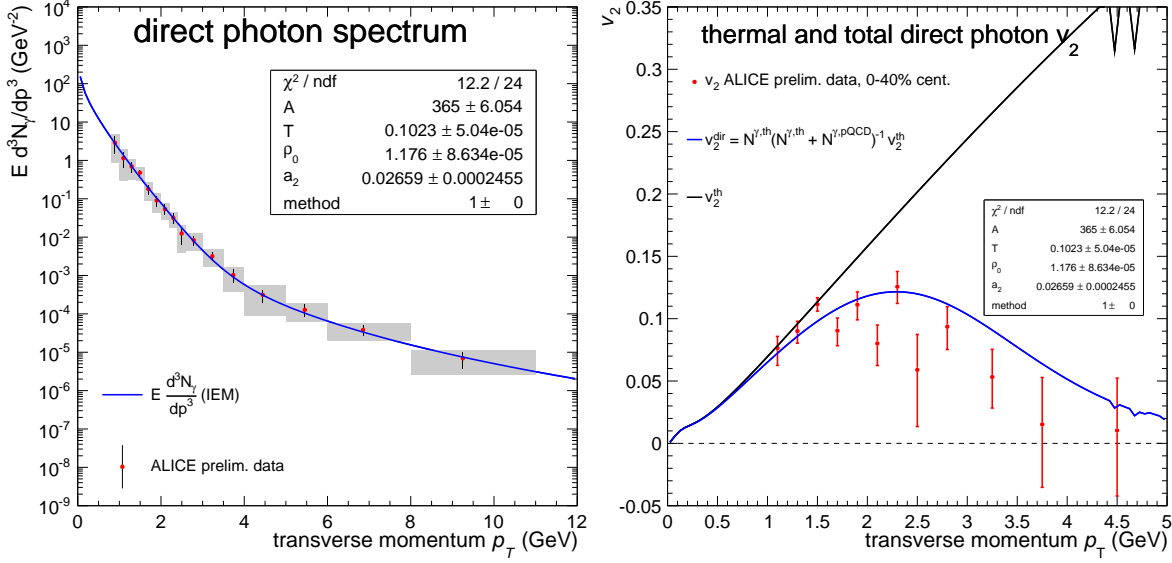


Figure 4.5: The direct photon spectrum (left) and v_2^{dir} spectrum (right) of the ALICE data are described well by the IEM.

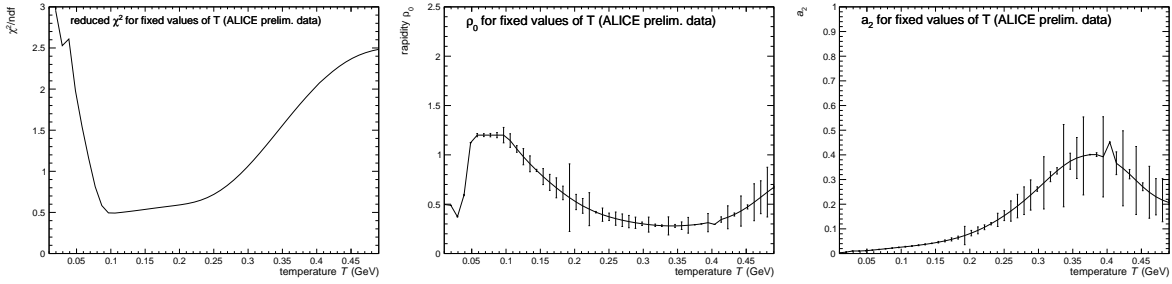


Figure 4.6: The χ^2 -values (top) of IEM fits with fixed temperature values to the ALICE data and the corresponding results for ρ_0 (middle) and a_2 (right) reveal the corresponding parameter freedom.

If one considers the minimal χ^2 values (see figure 4.7), one can see this confirmed, as the minimal χ^2 region does not extend to $\rho_0 = 0$. In comparison to the FEM, the ridge no longer runs through the bottom of the valley but instead seems to have moved to the high temperature side. Also, in the a_2 - T -plane, the region of best χ^2 values is smaller and only includes a_2 values between 0.03 and 0.18. The overall shape, though, is more or less like in the FEM.

In conclusion, it can be said that the IEM suggests a minimal rapidity and a maximum a_2 , although it describes the data slightly worse. The minimal rapidity could be taken as a sign that the photons stem from a phase with prevalent collective flow. It also provides an optimal fit at a single temperature, though admittedly the fits for the neighbouring

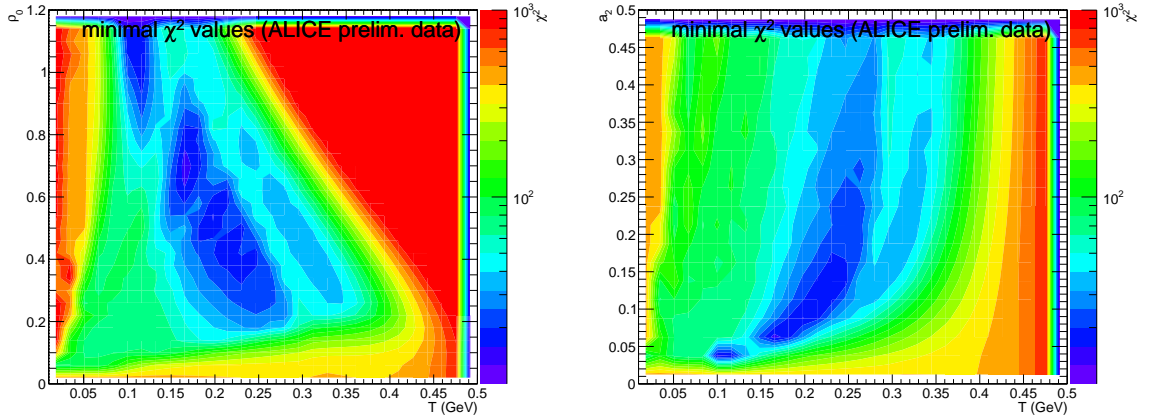


Figure 4.7: The minimal χ^2 values for parameter combinations of ρ_0 and T (left) as well as a_2 and T (right) illustrate the parameter freedom in the IEM description of the ALICE data.

higher temperatures are almost as good. So while there still is a big amount of parameter freedom, the parameters could also be clearly constrained more than in the FEM. Within the good fit regions, though, the differences between the descriptions of the data are not very large.

4.3 PHENIX Data

In order to see how the direct photon models can describe other data they were fitted to data from PHENIX⁴ measurements. The PHENIX data consist of direct photon invariant yields [24] and v_2^{dir} spectra [25] measured in gold-gold collisions with $\sqrt{s_{\text{NN}}} = 200$ GeV at RHIC. These data exist in three sets for minimum bias⁵ as well as for 0–20% and 20–40% centrality.

4.3.1 pQCD Contribution

In order to determine the factor $N_{\gamma}^{\text{th}}/N_{\gamma}^{\text{dir}}$, the invariant yield was compared to the scaled proton-proton data for each of the three centrality classes of the gold-gold collisions (see figure 4.8). The ratios of a modified power-law fit to the p+p data to the data of the gold-gold collisions correspond directly to one minus said factor. These ratios have then

⁴ The Pioneering High Energy Nuclear Interaction eXperiment (PHENIX) detector is one of the RHIC experiments at the BNL.

⁵ ‘Minimum bias’ here means that the data have not been constrained to a certain centrality class.

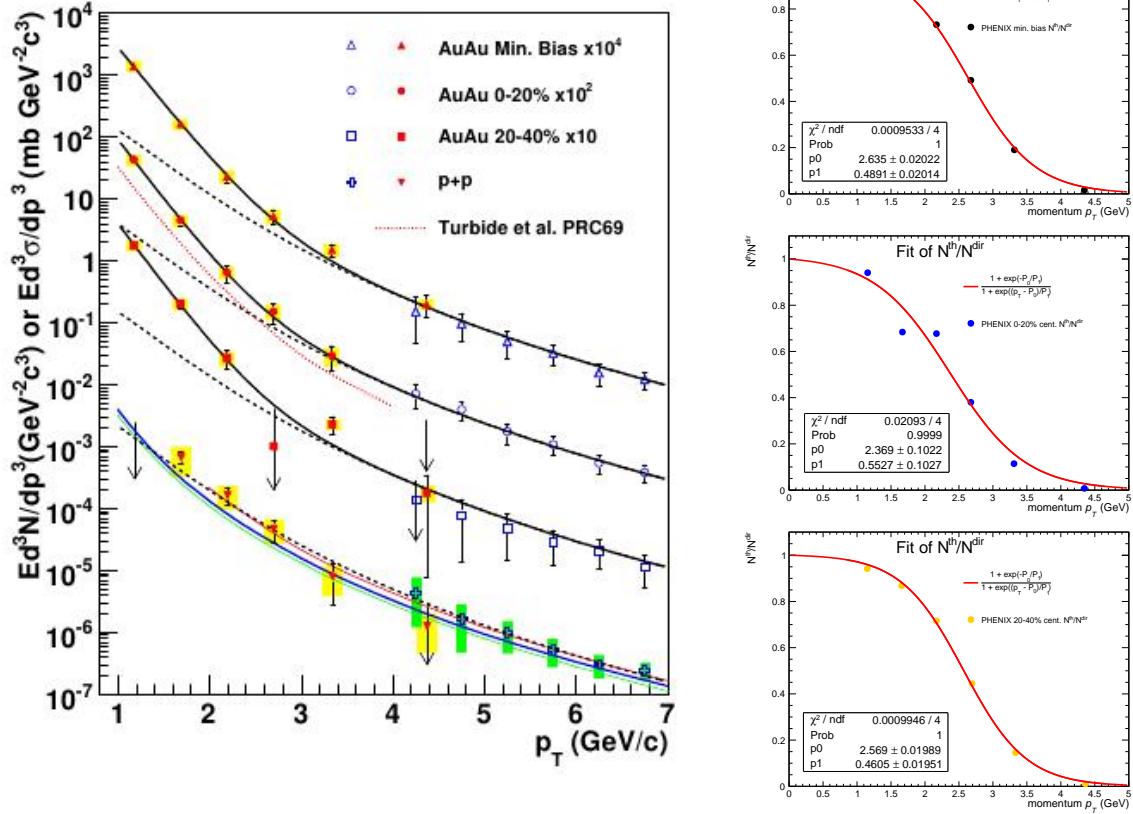


Figure 4.8: For the determination of the pQCD photon contribution, $N_{\gamma}^{\text{th}}/N_{\gamma}^{\text{dir}}$ has been calculated from the PHENIX data [24] (left) as one minus the ratio of the scaled p+p fit (dotted lines) to the invariant yield in gold-gold collisions and then fitted to the function in equation (3.7) for the min. bias data (top right) as well as for 0–20% (middle right) and 20–40% (bottom right) centrality.

been fitted to the function described in equation (3.7), which describes them very well (see figure 4.8 on the right). The fit results were $P_0 = 2.635$ GeV and $P_1 = 0.4891$ GeV for the minimum bias data, $P_0 = 2.369$ GeV and $P_1 = 0.5527$ GeV for 0–20% centrality, as well as $P_0 = 2.569$ GeV and $P_1 = 0.4605$ GeV for 20–40% centrality.

Now the contribution of the pQCD photons to the invariant yield had still to be added. The values have again been calculated and provided by Werner Vogelsang [23] for $p_T \geq 1.25$ GeV. They were then fitted to a Hagedorn function as in equation (4.2)), which lead to the results $h_0 = 0.1864$ GeV⁻², $p_0 = 0.4298$ GeV, and $n = 6.272$ (see figure 4.9), The fits describe the pQCD calculation very well up to above $p_T = 10$ GeV, which lies in turn well above the highest fitted invariant yield data point. Finally, in order

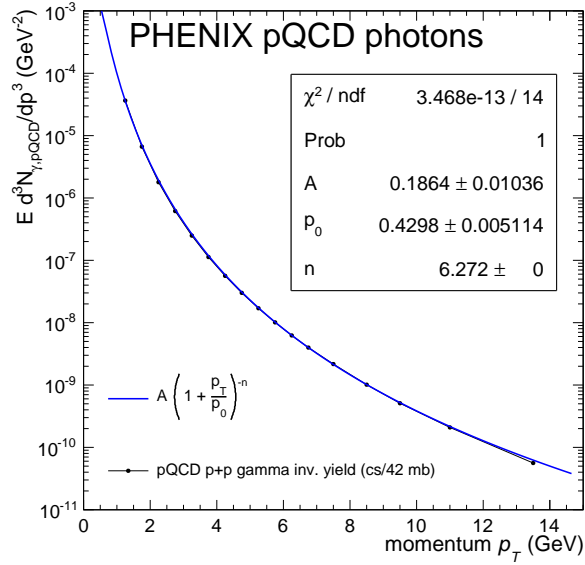


Figure 4.9: The Hagedorn function which describes the PHENIX pQCD photon calculation was in the following used to add the pQCD contribution to the invariant yield.

to account for the different centrality classes, h_0 had yet to be multiplied by the N_{coll} factors $N_{\text{coll}}^{\text{min. bias}} = 257.8$, $N_{\text{coll}}^{0-20\% \text{ cent.}} = 779.0$, and $N_{\text{coll}}^{20-40\% \text{ cent.}} = 296.8$, respectively.

4.3.2 Forward Emission Model

After fitting the FEM to the PHENIX data (see figure 4.10) one notices mainly two things: On the one hand, the direct photon spectra for all three spectra are fitted rather well. Only at higher transverse momenta one notices small deviations for single data points. On the other hand, the v_2^{dir} spectra are not described very good. While the systematic deviations for the minimum bias data are mostly only about the size of the statistical errors, they are still recognisable as such.

The deviations for the 0–20% and 20–40% centrality are even larger. In particular, the fits mainly overshoot the data for low $p_T \lesssim 2 \text{ GeV}$ and undershoot it for higher p_T . So all in all the PHENIX data are not described very well by the FEM.

4.3.3 Isotropic Emission Model

In contrast, the IEM fits to the PHENIX data are considerably better, as can be seen in figure 4.11. While the invariant yields are described as good as with the FEM, the v_2^{dir}

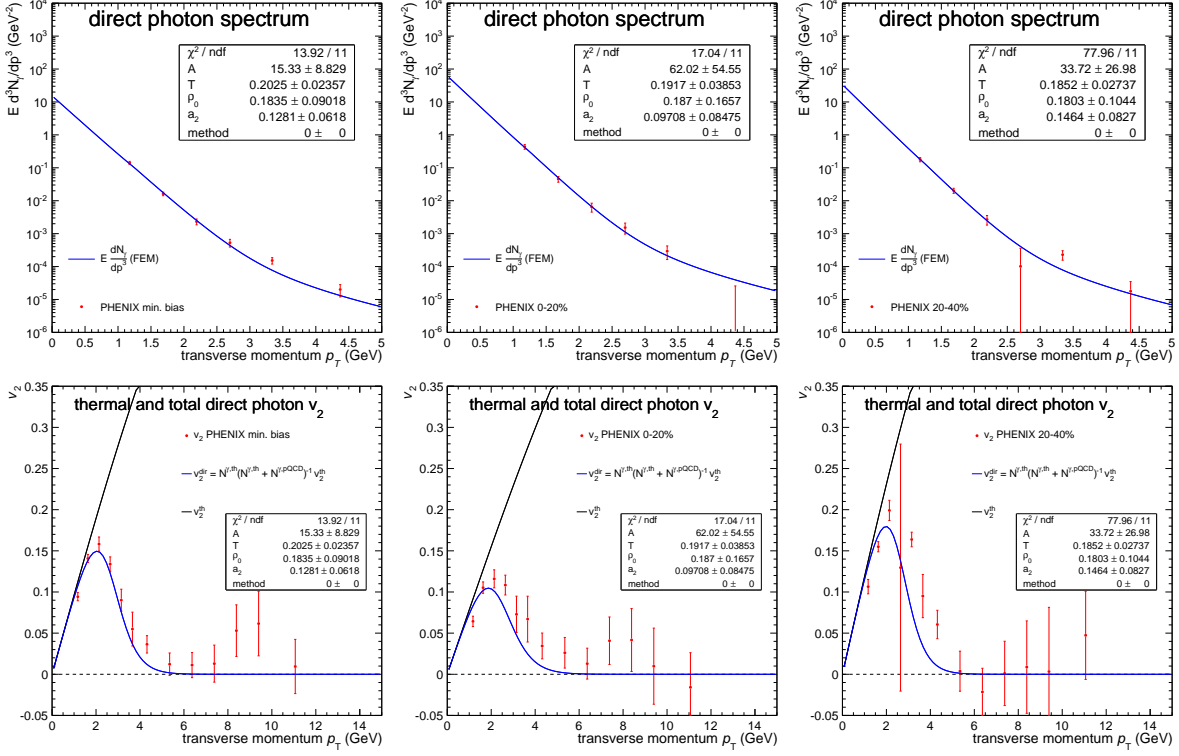


Figure 4.10: The direct photon spectra (top) of the PHENIX min. bias (left), 0–20% (middle) and 20–40% centrality (right) data are fitted quite well by the FEM, unlike the v_2^{dir} spectra (bottom).

centrality class	T_0 (GeV)	T_{min} (GeV)	T_{max} (GeV)	ρ_0^{max}	ρ_0^{min}	a_2^{min}	a_2^{max}
min. bias	0.18	0.08	0.22	1.2	0.3	0.02	0.21
0–20%	0.21	0.08	0.29	1.2	0.13	0.02	0.5
20–40%	0.19	0.115	0.26	0.85	0.1	0.05	0.5

Table 4.1: The IEM fits with fixed temperature values as shown in the plots in figure 4.12 are optimal in regions around the minimum T_0 between T_{min} and T_{max} . The fits within those regions cover rapidities roughly between ρ_0^{max} and ρ_0^{min} as well as a_2 values between a_2^{min} and a_2^{max} .

values of the minimum bias and 0–20% centrality data are described almost exactly up to a transverse momentum of about 4 GeV. The v_2^{dir} spectrum of the 20–40% centrality data still shows systematic deviations especially for higher $p_T \geq 3$ GeV, but is still described significantly better than in the FEM.

To examine the parameter freedom, one can again look at the fit results for fixed temperature values (see figure 4.12). The χ^2 values have temperature regions where

4 Fits to Various Data Sets

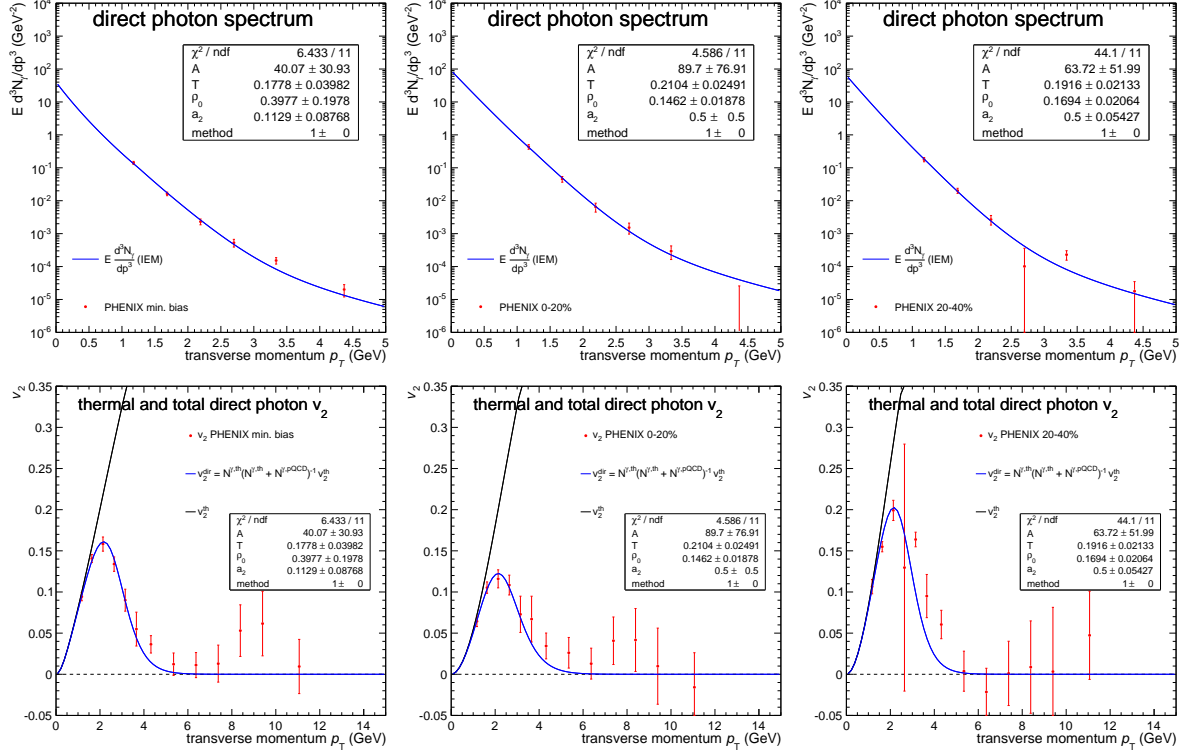


Figure 4.11: The direct photon (top) and v_2^{dir} spectra (bottom) of the PHENIX min. bias (left) and 0–20% centrality (middle) data are described very well by the IEM fits. The 20–40% centrality data (right) is described considerably better than in the FEM.

they are optimal around a minimum at the temperature T_0 . Within these regions the rapidity ρ_0 drops from a maximum to a minimum value, while the rapidity modulation strength parameter a_2 increases. The respective values are provided in table 4.1.

If now the minimal χ^2 values for different parameter combinations are looked at as in figure 4.13, one can study the parameter freedom from another angle. The ρ_0 - T plot for the minimum bias data shows good fit regions that remotely resemble two valleys divided by a small ridge that are crossed by a bigger ridge and some smaller ones. This leads to several islands of low χ^2 for $0.12 \text{ GeV} \lesssim T \lesssim 0.24 \text{ GeV}$ and $0.2 \lesssim \rho_0 \lesssim 0.6$ as well as another island at higher rapidity $0.8 \lesssim \rho_0 \lesssim 1.05$ and lower temperature $T \approx 0.1 \text{ GeV}$.

The good fit regions in the a_2 - T plot resemble two valleys divided by a ridge, too. In general all a_2 values between 0.05 and 0.25 seem to be contained in these regions for temperatures between 0.1 GeV and 0.24 GeV.

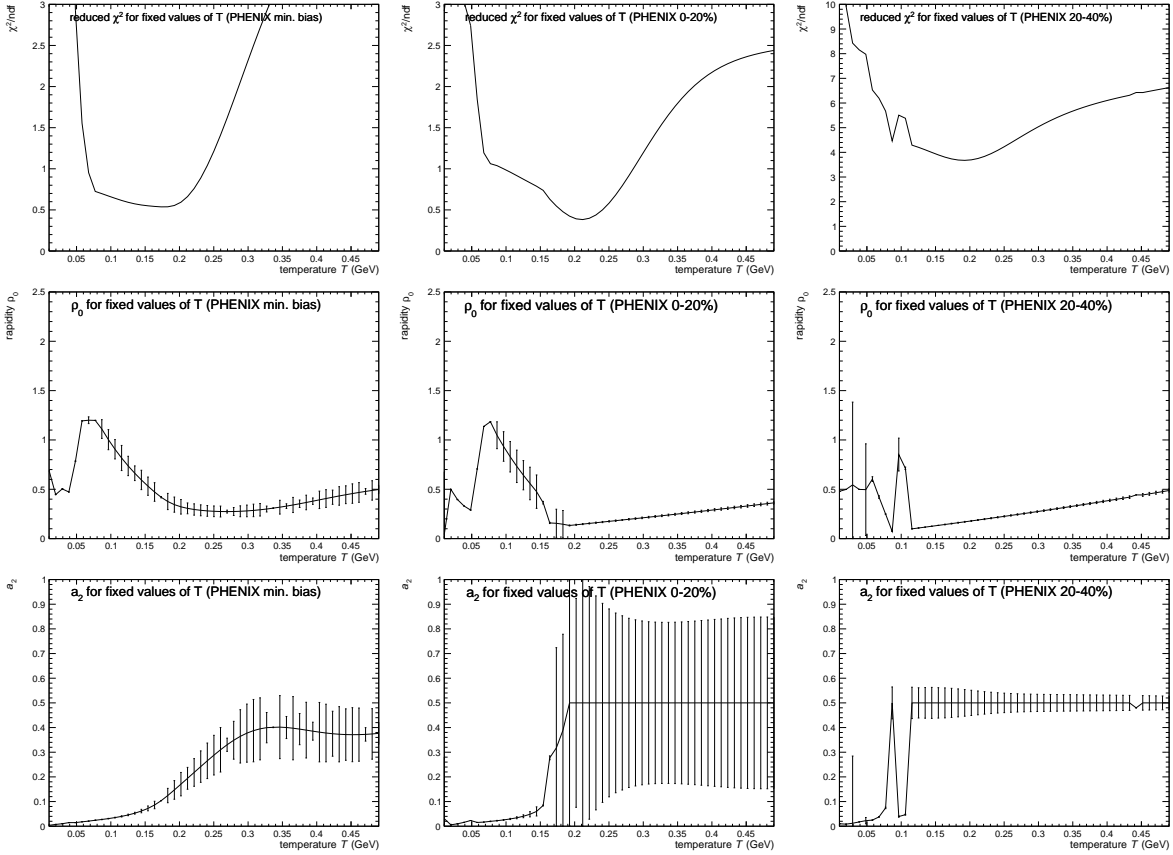


Figure 4.12: The χ^2 values (top) of IEM fits for fixed temperatures with their corresponding ρ_0 (middle row) and a_2 (bottom) values show the parameter freedom for the PHENIX min. bias (left), 0–20% (middle column) and 20–40% (right) centrality data.

In the respective plots for 0–20% centrality the overall shape is similar, but the optimal χ^2 values are constrained to smaller regions in the ρ_0 - T plot between $T \approx 0.15$ GeV and $T \approx 0.15$ GeV, which corresponds to the rapidities $0.15 \lesssim \rho_0 \lesssim 0.55$. These optimal fit regions cover also most a_2 values between 0.05 and 0.5. Other good fit regions in the ρ_0 - T plot with somewhat higher χ^2 values correspond largely to the good fit regions for the minimum bias data, but extend to higher temperatures up to $T \approx 0.3$ GeV.

The regions of good χ^2 values for 20–40% centrality look similar, but are more irregular. The optimal fits seem to be confined to a smaller rapidity region around $\rho_0 \approx 0.2$. One also notices that the χ^2 values for 0–20% centrality are generally slightly lower than their minimum bias counterparts, while the values for 20–40% centrality are higher, which represents the on the whole worse fits for this centrality class. It is also noticeable that the good fit regions do not extend to vanishing rapidities, which could be a sign of a collective flow.

4 Fits to Various Data Sets

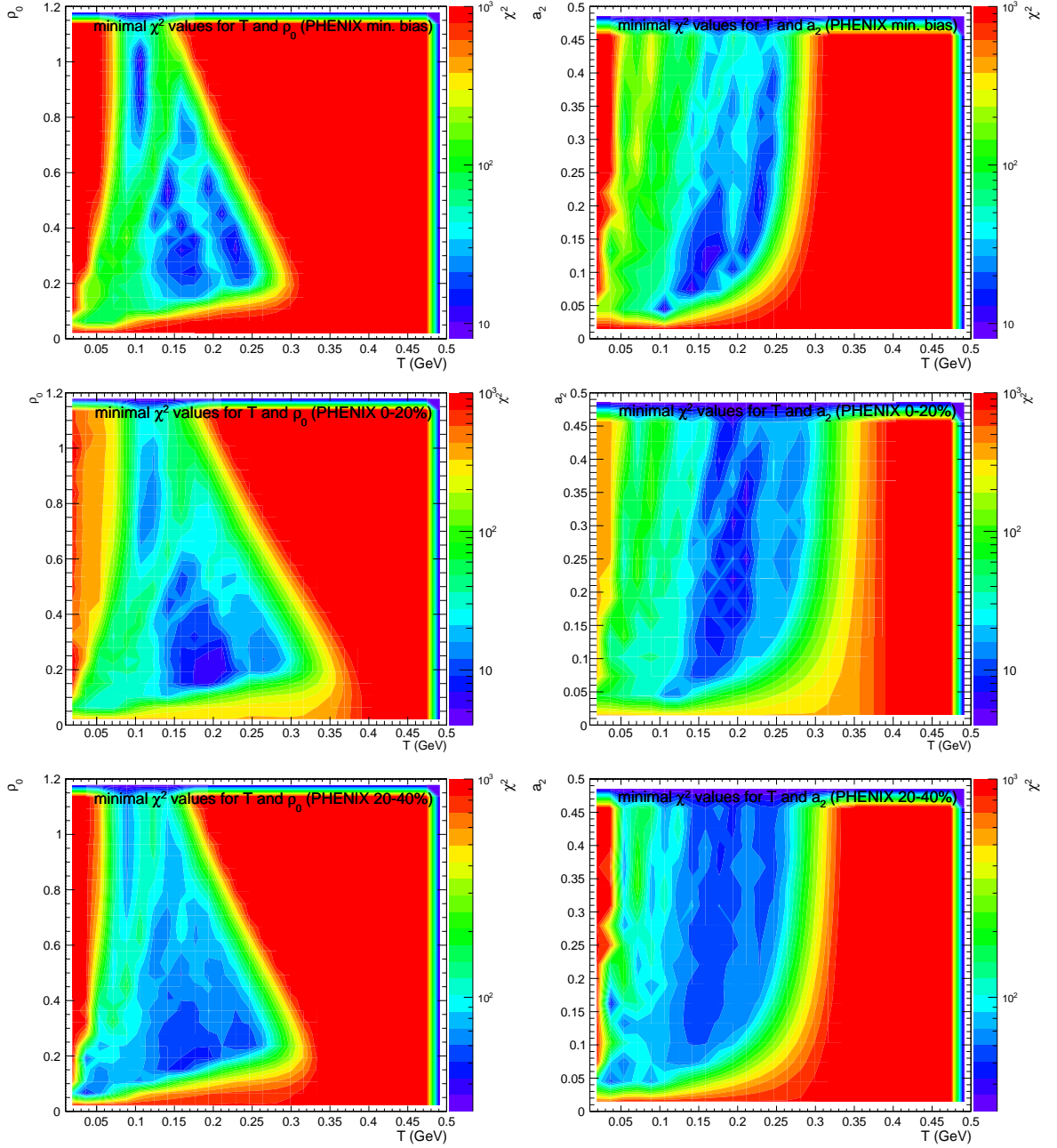


Figure 4.13: Minimal χ^2 values for parameter combinations of ρ_0 and T (left) as well as a_2 and T (right) for PHENIX min. bias (top), 0–20% (middle) and 20–40% (bottom) centrality data illustrate the parameter freedom in the IEM.

In conclusion, the PHENIX data sets are described very well by the IEM, or, in the case of 20–40% centrality, at the very least significantly better than in the FEM. While the parameters parameter freedom is still not negligible, it is smaller than it was for the ALICE data.

4.4 WA98 Data

The next data that have been fitted were the WA98 data [26], which consist of a direct photon spectrum measured in $^{208}\text{Pb}+^{208}\text{Pb}$ collisions at 158 A GeV, carried out at the CERN WA98 experiment. This data set also includes two data points at very low p_T with an invariant yield significantly higher than the theoretical prediction [27]. Therefore the IEM was fitted to the data in order to check whether those two points could be explained as a result of redshift.

Because the experimental data encompassed only the invariant yield and not the v_2^{dir} , only the direct photon spectrum was used for the fit. For the same reason the parameter a_2 was fixed to zero⁶, so that the resulting velocity only depended on ρ_0 .

As one can see in an exemplary fit in figure 4.14, however, the redshift in the IEM is not sufficient to explain why the two values at very low p_T are so large. Apart from that, though, the remaining data points are fitted very well. The upper limits, which were not used for the fit, are also never overshoot.

4.5 Theoretical Hydrodynamical Calculations

After the ALICE data were described relatively well by the FEM as well as the IEM and the IEM did a very good job of describing the PHENIX data, it was of interest to see how those two models would compare against more complex theoretical calculations. Holopainen et al. did ideal-hydrodynamical calculations of the thermal photon transverse momentum spectra and elliptic flow for Pb+Pb collisions at $\sqrt{s_{\text{NN}}} = 2.76$ TeV at the LHC [28], which they provided for 0–40% centrality and with ‘wash-out’⁷ of thermal v_2^{th} into direct photon v_2^{dir} [29]. Since the calculations were done for thermal photons, they

⁶ Control fits with a_2 unfixed always resulted in very small values for a_2 as well. Therefore fixing a_2 did not impact the fit results, but still reduced the computation time.

⁷ ‘Wash-out’ refers to the assumption that the difference between the measured direct photon yield and the calculated thermal photon yield stems from sources with $v_2 = 0$.

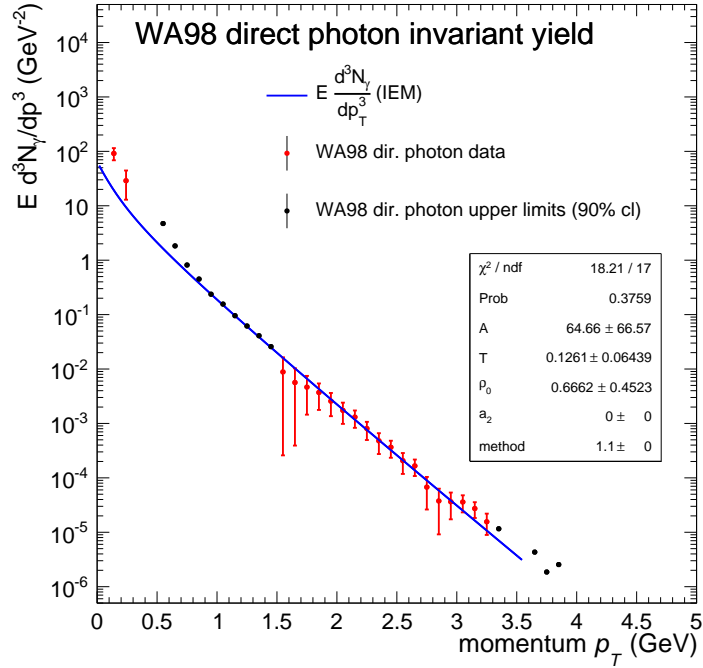


Figure 4.14: The redshift in the IEM is not sufficient to explain the two WA98 data points at very low p_T , but the rest of the spectrum is described very well.

were fitted without the pQCD contribution in the linear range of the calculations up to $p_T \approx 1$ GeV.

The theoretical values stem from three slightly different calculations. “L170TRG” refers to calculations assuming a lattice equation of state and a critical temperature of $T_c = 170$ MeV. “L200TRG” is similar, except that $T_c = 200$ MeV. Finally, “Q165R92” assumes a bag equation of state and $T_c = 165$ MeV. The endings “TRG” and “R92” refer to different hadron gas emission rates.

4.5.1 Forward Emission Model

Figure 4.15 shows exemplary fits of the thermal FEM to the three calculations. As can be seen, the direct photon spectra agree for low p_T up to little above 1 GeV. Then the invariant yields in the hydrodynamical calculations start to decrease much slower than in the FEM.

The v_2^{th} values are also similar up to slightly below 1 GeV, where the calculated thermal elliptic flow starts to first grow slower, and then decreases from about $p_T \approx 1$ GeV. In both cases the differences could be explained by the fact that Holopainen et al. assume

4.5 Theoretical Hydrodynamical Calculations

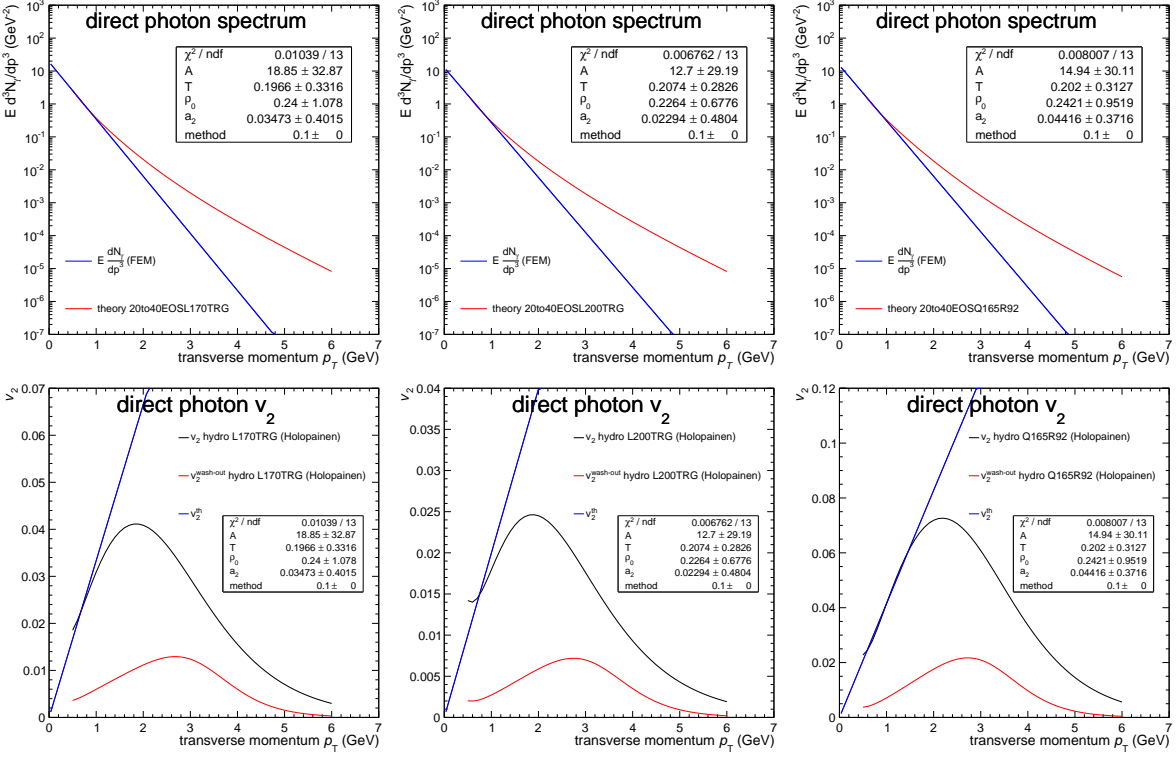


Figure 4.15: Holopainen’s hydrodynamical calculations L170TRG (left), L200TRG (middle) and Q165R92 agree with the FEM very well for low transverse momenta, but not for high p_T .

a hydrodynamically interacting system and describe the spacetime evolution of the system, while the FEM and IEM assume a static system.

One peculiar detail is that the theory calculations do not seem to head exactly towards $v_2(p_T = 0) = 0$ like the FEM, which would normally be expected. However, it is difficult to assess, because the v_2 calculation values start only at about 0.5 GeV. In general the deviations seem to be smallest for the Q165R92 values and largest for the L200TRG values, although the differences are small. The significance of the differences between the calculation and the fit is also difficult to judge since there were no errors provided for the calculation.

All in all the FEM does not describe Holopainen’s hydrodynamical calculations very well, although the differences are very small at low p_T . Otherwise they can be explained by the fact that the theoretical calculations by Holopainen include the description of a spacetime evolution.

4 Fits to Various Data Sets

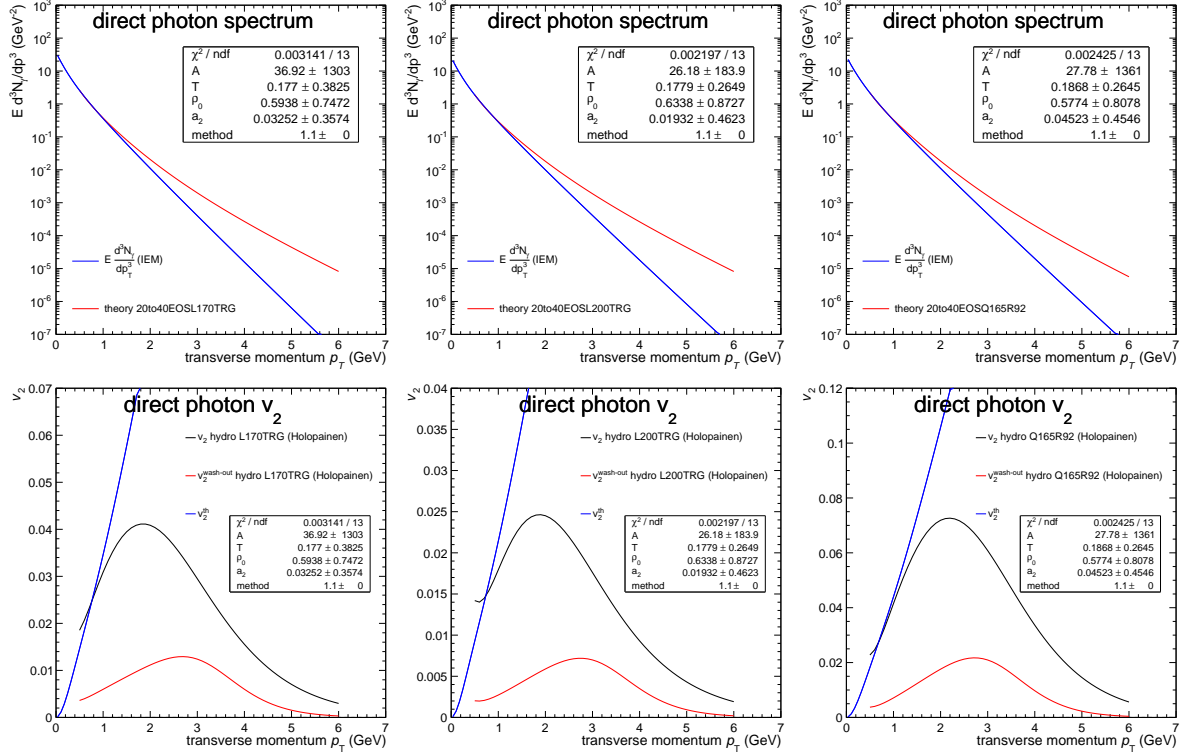


Figure 4.16: Holopainen's hydrodynamical calculations L170TRG (left), L200TRG (middle) and Q165R92 (right) agree very well with the IEM for low p_T only.

4.5.2 Isotropic Emission Model

In principle, the same can be said about the fits of the IEM to Holopainen's hydrodynamical calculations (see figure 4.16). However, the invariant yields now agree very well up to about $p_T = 1.5$ GeV.

In conclusion, both the FEM and the IEM fail to reproduce the spectra of Holopainen's hydrodynamical calculations exactly. This is no big surprise, as the theoretical calculations include a description of the spacetime evolution of the system. Still, both the FEM and the IEM provide a fairly good approximation of the more complex model calculations at lower transverse momenta.

4.6 ALICE π^\pm Data

Finally, the last data set that was fitted consisted of the invariant yield [30] and elliptic flow [31] of charged pions measured by ALICE at CERN in $\sqrt{s_{NN}} = 2.76$ TeV Pb-Pb collisions for 0–40% centrality. Since these parameters are the same as for the measure-

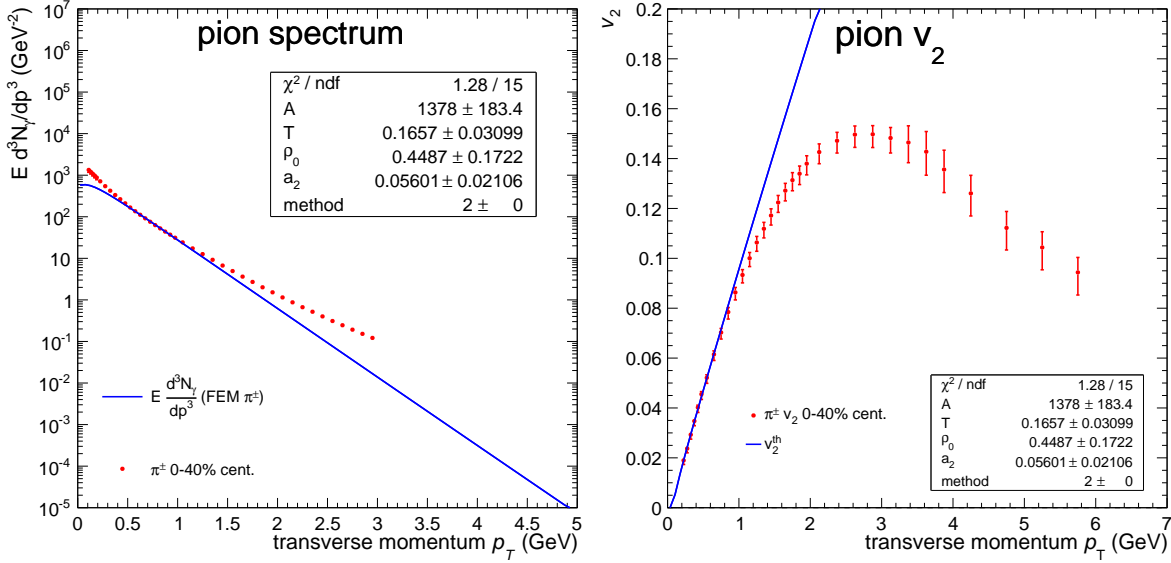


Figure 4.17: The ALICE π^\pm data were fitted with the modified FEM to accommodate for the pions' non-zero rest mass. The data are described well within the fit regions of $0.5 \text{ GeV} \leq p_T \leq 1 \text{ GeV}$ for the invariant yield and $0 \text{ GeV} \leq p_T \leq 0.8 \text{ GeV}$ for v_2^{th} .

ment of the direct photon ALICE data, whose fits were described in section 4.2, the two measurements could be easily compared.

For the charged pions, like all hadrons originating from the ion collisions, it can be assumed that the average rapidity with which they get boosted is the final rapidity during the freeze-out of the hadron gas, because, unlike the photons', their mean free path is too small to let them cross the fireball unobstructed. If the photons actually arise mainly in a later phase of the spacetime evolution of the QGP and hadron gas, this final rapidity would be the maximum rapidity with which they could be boosted. Consistent fit results for the ALICE charged pions and photons would then mean that this hypothesis cannot be ruled out, at least based on the models used in this thesis.

As the charged pions are not assumed to be able to cross the HG after their formation during freeze-out and have a rest mass of $m_{\pi^\pm} \simeq 0.13957 \text{ GeV}$ [32], the FEM for massive particles was used for the fits to the data. For very low p_T values resonances occur and for high p_T pQCD effects dominate over the thermal pions. In addition, the ratio between the thermal and the direct photons was not known, so that the data have only been fitted with the thermal invariant yield and elliptic flow parameter v_2^{th} . Therefore the fits have been carried out for $0.5 \text{ GeV} \leq p_T \leq 1 \text{ GeV}$ for the thermal invariant yield and $0 \text{ GeV} \leq p_T \leq 0.8 \text{ GeV}$ for v_2^{th} . It should be kept in mind that the choice of these

4 Fits to Various Data Sets

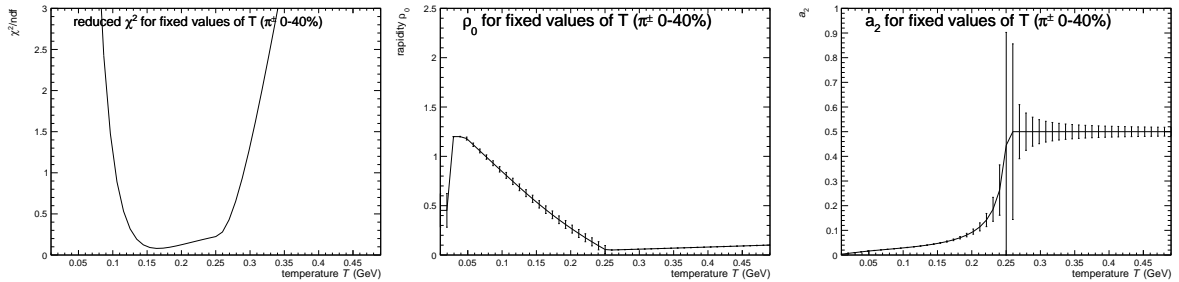


Figure 4.18: Fixed temperature fits and the resulting χ_{red}^2 (left), ρ_0 (middle) and a_2 (right) values show the parameter freedom for the fits of the modified FEM to the π^\pm data.

fit regions was a rough estimation based on where the data followed more or less an exponential spectrum. Different regions might have lead to quite different fit results as well.

An exemplifying fit can be seen in figure 4.17. Unsurprisingly, the modified FEM describes the data very well in the fit region, because they have been chosen in such a way that it would be possible to describe the data by a purely thermal distribution. Up to about 1.5 GeV the invariant yield data points are described fairly well by the fit. However, the π^\pm data decrease increasingly slower than the exponential FEM for massive particles. Below 0.5 GeV the resonances lead to a steeper shape of the data, while the effect of the charged pion rest mass m_{π^\pm} becomes noticeable, which manifests itself in a flatter fit curve towards $p_T = 0$.

The charged pion v_2 data points start at about 0.9 GeV to fall below the FEM curve and reach a maximum at about 3 GeV, from where they begin to decrease. However, the data points decrease much slower than they did for the direct photon v_2 .

Just like for the other data sets, the parameters of the fits to the π^\pm data have a lot of freedom. The results for fits with fixed temperature values between $T = 0.01$ GeV and $T = 0.5$ GeV are shown in figure 4.18. A region of minimal χ_{red}^2 values lies between the temperatures of 0.13 GeV and 0.26 GeV, in which the corresponding rapidity values drop from 0.65 to its minimum value of about 0.05 and a_2 increases from 0.04 to the parameter constraint of 0.5. However, even for $0.105 \text{ GeV} \lesssim T \lesssim 0.29 \text{ GeV}$ the χ_{red}^2 values don't exceed 1, while $0.05 \lesssim \rho_0 \lesssim 0.8$ and $0.03 \lesssim a_2 \leq 0.5$.

Figure 4.19 shows an overview over the minimal χ^2 values for the π^\pm data for various parameter combinations. The good fit regions for combinations of ρ_0 and T consist of islands of low χ^2 along a more or less straight band that cover most of the temperatures

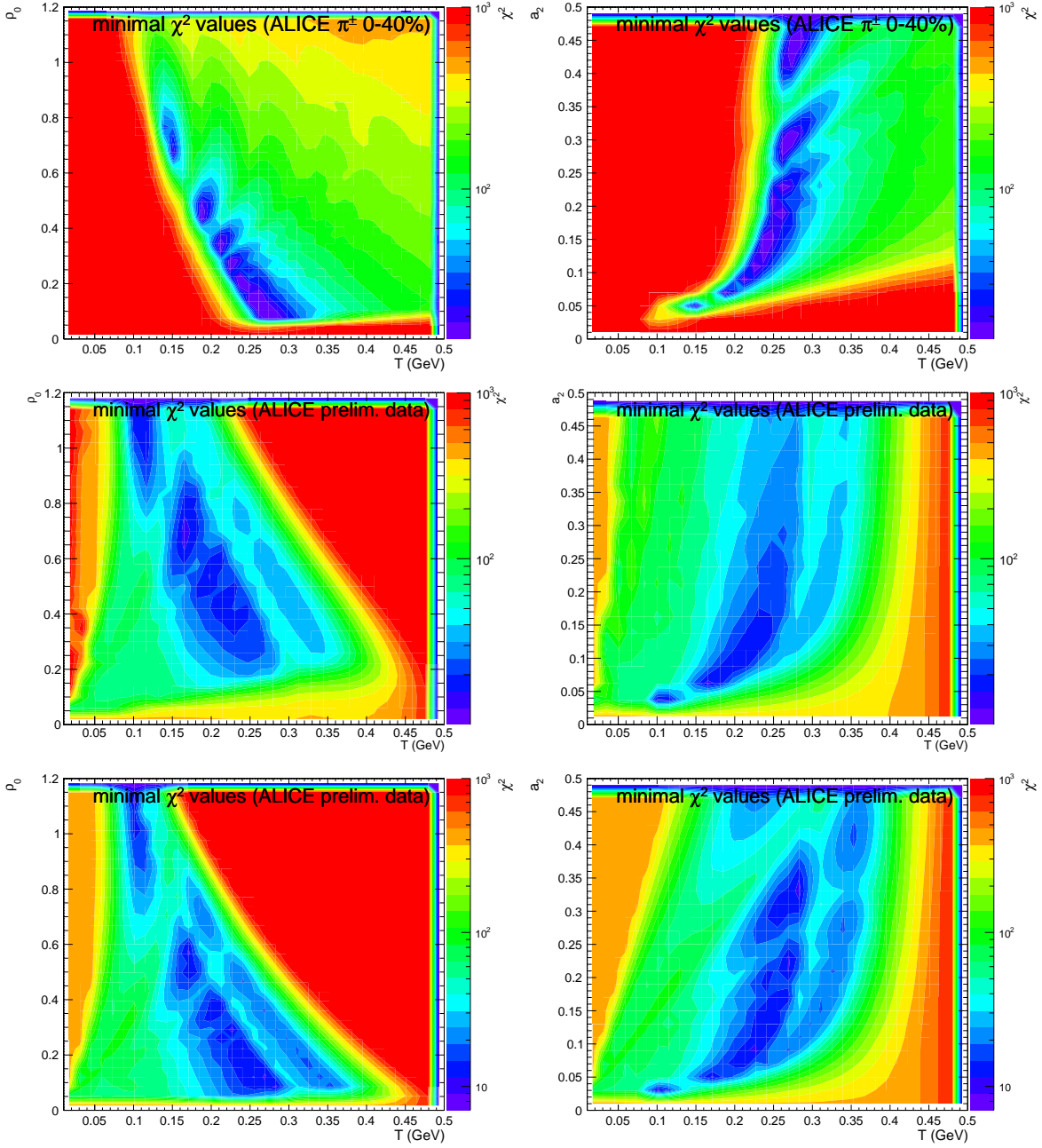


Figure 4.19: The minimal χ^2 values for parameter combinations of ρ_0 and T (left) as well as a_2 and T show the parameter freedom of the fits of the modified FEM to the π^\pm ALICE data (top). These good fit regions lie partly within those of the IEM (middle), and mainly within those of the FEM (bottom) fits to the ALICE direct photon data.

between 0.14 GeV and 0.32 GeV, and rapidities between about 0.06 and 0.8. Similarly, in the a_2 - T plane most a_2 values from about 0.05 up to 0.5 are covered by islands of minimal χ^2 within the same temperature range.

In conclusion, the ALICE charged pion data can be described quite well within its fit regions. The parameters still have a considerable amount of freedom, however, even though it is smaller than for the ALICE direct photon data.

In figure 4.19 the minimum χ^2 values of the fits to the ALICE direct photon data described in section 4.2 are shown as well for comparison. One finds that the good fit regions of low χ^2 values for the π^\pm data between $T \approx 0.18$ GeV and $T \approx 0.25$ GeV as well as $\rho_0 = 0.25$ and $\rho_0 = 0.55$ lie within the optimal χ^2 regions of the IEM fits to the direct photon data. The smaller good π^\pm fit region at about $T \approx 0.15$ GeV also lies within the good IEM fit regions. The good parameter regions of the π^\pm fits up to $T \approx 0.25$ GeV and $a_2 \approx 0.175$ also lie within the optimal IEM fit regions in the a_2 - T plot, while the remaining combinations of a_2 and T still correspond to mostly good IEM fit regions.

Regarding the agreement between the values for the FEM fits to the direct photon data and the π^\pm data, one notices that there the coinciding good fit regions extend up to $T \approx 0.3$ GeV. However, the low χ^2 islands of the π^\pm fits at $T \approx 0.15$ GeV and $\rho_0 \approx 0.7$ as well as those with $a_2 \gtrsim 0.4$ do not lie within the optimal fit regions of the corresponding direct photon data plot.

This means that there are parameter regions which explain both the ALICE direct photon and charged pion data simultaneously. In turn, this implies that the assumption that direct photons arise mainly in a later phase of the fireball with a large collective flow gives rise to a consistent description of the data for both the FEM and the IEM.

If one now wishes to further constrain the possible parameter combinations one can take into considerations that the charged pions do not form prior to the HG stage of the system evolution. Therefore the inverse slope parameter T of their spectrum can be assumed to lie somewhere between T_c and T_{fo} , i.e. $0.1 \text{ GeV} \lesssim T \lesssim 0.15 \text{ GeV}$. According to the charged pion fits this implies an a_2 not higher than 0.05. Since the a_2 of the photons should not be larger than that of the pions, this corresponds to direct photon fits with $0.1 \text{ GeV} \lesssim T \lesssim 0.2 \text{ GeV}$ and accordingly rapidities between about 0.4 and 1.2 for the optimal fit regions. In any case, this indicates that the photons indeed stem from a source with a considerable collective flow.

5 Outlook

In the previous chapter it was shown that the three models presented in chapter 3 do a reasonable job at describing the direct photon data from ALICE and PHENIX as well as the thermal charged pions from ALICE. However, their limitations due to their simple design became apparent as well. Plus, the model fits all showed big amounts of parameter freedom and did not allow the pinpointing of unique parameter combinations describing the data. In particular, this meant that no definitive conclusions could be drawn regarding the initial temperature and mean rapidity of the QGP respectively of the HG.

In order to improve the fits and the significance of their results, there are many different paths one could choose. One would be to try to fit more data from the same collisions, e.g. for different types of hadrons, to see whether a consistent description would be possible and to further narrow down the good fit regions. However, it is possible that the main difficulties of the models, i.e. the inability to conclusively find distinct minima, would not vanish this way, but only be cushioned.

Another obvious choice would therefore be to enhance the model to a more complex, but also more accurate description of the physical system. For example, one could include different values of the same measurements, like the triangular flow parameter v_3 , into the selection of data that is fitted simultaneously. While this might only call for a small modification of the models, it also gives an additional free parameter that has to be fitted.

One huge simplification is the assumption of a static system, which is in stark contrast with the physical reality. This means that the fit parameters used are merely effective time averages, while they in fact change with time. For this reason a model involving a time evolution of the system has been planned, which could unfortunately not be implemented during the limited time span of this bachelor thesis.

5.1 Time Evolution Model

Contrary to the previous static models, this model assumes a system that evolves with the eigentime τ . In particular, the system starts as a thermalised QGP at τ_0 , and then expands and cools until it reaches the critical temperature T_c at the eigentime τ_c , at which it undergoes a first order phase transition to a HG until $\tau = \tau_c + \Delta\tau_c$. The system then continues expanding and cooling as a HG, until it reaches the freeze-out temperature T_{f_0} at τ_{f_0} .

During this evolution it is assumed that the entropy $S = S_0$ stays constant, which means that the entropy density $s = \frac{S_0}{V(\tau)}$ develops like the inverse of the volume $V(\tau)$. The volume of the system depends on a longitudinal expansion along the beam axis \vec{e}_z and a transversal expansion.

For the longitudinal expansion $z(\tau)$ a Bjorken flow with $\beta_z \approx 1$ is assumed, which means that $z(\tau) = \tau$. For the radial expansion one assumes an initially anisotropic surface $R(\varphi, \tau) = R_0 \cdot (1 - k_r \cos(2\varphi))$, which is initially not changing, i.e. $\frac{\partial}{\partial \tau}(R(\varphi, \tau_0)) = 0$. The anisotropy parameter k_r is chosen between 0 and $\frac{1}{4}$, so that the resulting surface is roughly elliptic or reminiscent of the collision zone in a central collision. Afterwards the radial surface is assumed to expand with a constant, anisotropic acceleration $a_S(\varphi) = a_0 \cdot (1 + 2a_2 \cos(2\varphi))$. All in all, this means that the radial surface evolves like $R(\varphi, \tau) = R(\varphi, \tau_0) + \frac{1}{2}a_S(\varphi) \cdot \tau^2$ for $\tau \geq \tau_0$ and therefore the volume as follows:

$$\begin{aligned} V(\tau) &= z(\tau) \cdot A_r(\tau) = \tau \int_0^{2\pi} d\varphi \int_0^{R(\varphi, \tau)} r dr = \frac{\tau}{2} \int_0^{2\pi} d\varphi R^2(\varphi, \tau) \\ &= \frac{\pi}{4} a_0^2 (1 + 2a_2^2) \tau^5 + \pi R_0 a_0 (1 - k_r a_2) \tau^3 + \frac{\pi}{2} R_0^2 (2 + k_r^2) \tau. \end{aligned} \quad (5.1)$$

The next assumption is that the QGP is ideal, which implies that the entropy density s is proportional to the cube of the temperature T , i.e. $s = \frac{2\pi^2}{45} g_{\text{phase}} T^3(\tau)$, where g_{phase} depends on the number of degrees of freedom of the system. It is often assumed to be $g_{\text{QGP}} = 42.5$ in a QGP with two and a half effective quark flavours and $g_{\text{HG}} \approx 12$ in a HG [33]. From there it follows that the temperature evolves like

$$T(\tau) = \sqrt[3]{\frac{45}{2\pi^2} \frac{S_0}{g \cdot V(\tau)}}. \quad (5.2)$$

During the phase transition with $\tau_c \leq \tau \leq \tau_c + \Delta\tau_c$ the temperature stays constant at $T(\tau) = T_c$.

For the collective flow in the system it is assumed that its velocity β increases linearly with $r = \sqrt{x^2 + y^2}$ until it reaches its maximum at $R(\varphi, \tau)$, so that

$$\beta(r, \varphi, \tau) = \frac{r}{R(\varphi, \tau)} \cdot a_S(\varphi) \cdot \tau. \quad (5.3)$$

Finally, one assumes that the expanding system emits photons isotropically at every infinitesimally small point as in equation (3.10). However, now the normalisation factor A is assumed to be proportional to the temperature squared, i.e. $A(\tau) = A_0 \left(\frac{T(\tau)}{T_0}\right)^2$. Then the total spectrum can be calculated as

$$E \frac{d^3 N_\gamma}{dp^3}(p_T) = \int_{\tau_0}^{\tau_{\text{end}}} d\tau' \tau' A(\tau) \int_0^{2\pi} d\varphi \int_0^{R(\varphi, \tau')} r dr \int_0^{2\pi} d\theta \exp\left(-\frac{p_T}{T(\tau')} \cdot \frac{1 - \cos(\varphi - \theta) \cdot \beta(r, \varphi, \tau')}{\sqrt{1 - \beta^2(r, \varphi, \tau')}}\right), \quad (5.4)$$

where the additional factor of τ' stems from the integration over $z(\tau') = \tau'$.

Now one has to choose the right initial parameters. For some, these are roughly known from measurements or physical considerations, like e.g. R_0 , T_c , or T_{f_0} . For others, like the entropy, one has to make additional assumption. Common assumptions here are that S_0 is about 4 times the number of produced hadrons, i.e. $\left.\frac{dS}{dy}\right|_{y=0} = 4 \cdot \left.\frac{dn}{dy}\right|_{y=0}$, and that the entropy density $s = \left.\frac{dS}{dy}\right|_{y=0} \cdot \frac{1}{A_{\text{col}} \cdot \tau}$, where A_{col} denotes the area of the collision zone. This implies an initial temperature

$$T_0 = T(\tau_0) = \sqrt[3]{\left.\frac{dn}{dy}\right|_{y=0} \frac{90}{\pi^2} \frac{1}{g_{\text{QGP}} A_{\text{col}} \tau_0}}, \quad (5.5)$$

which lies at about 367 MeV for $\left.\frac{dn}{dy}\right|_{y=0} = \frac{3}{2} \cdot 1600$, $A_{\text{col}} = \pi(5 \text{ fm})^2$, and $\tau_0 = 1 \text{ fm}$.

Apart from finding the right initial parameters, the large computation time that can be expected from a quadruple integral could also pose a challenge. However, this model provides a reasonably accurate description of the physical reality, while still being less complex than full hydrodynamical or similar calculations, which should make the eventual results very interesting.

6 Conclusions

This bachelor thesis aimed at calculating direct photon spectra alongside their elliptic flow by means of simple, phenomenological models of a QGP respectively HG. In the end this should shed light on the question of whether or not an unexpectedly high direct photon elliptic flow in recent measurements [5] could be due to the photons being emitted mainly in later stages of the system, in which a collective hadron flow is prevalent. The general model expectation, on the other hand, had been that the direct photons arise mostly in the early hot plasma phase.

For this purpose two simple phenomenological models describing the direct photon invariant yield and the elliptic flow parameter v_2^{dir} simultaneously were designed, of which one, the IEM, was a slightly more complex advancement of the other, the FEM. An additional model was devised as a modification of the FEM in order to describe the thermal invariant yield and collective flow of massive hadrons.

These models were then fitted to several data sets, namely measurements from ALICE, PHENIX, and WA98. In addition, the models were compared to theoretical hydrodynamic calculations by Holopainen et al., which exemplified the limitations of the models due to their simplicity. The fits described the respective spectra usually very well, at the very least in the lower transverse momentum region. However, they also usually showed a big amount of parameter freedom, i.e. the fit results depended on the start values and did not converge conclusively to a single parameter combination. Consequently, the parameter freedom of the fits was examined for the different data sets. This showed that in each case many different combinations of the temperature, the collective flow rapidity, and its modulation strength could explain the data. However, the IEM fits also implied a minimum rapidity significantly above zero.

Furthermore, the ALICE direct photon data was compared to the charged pion data from the same measurements. This gave reason to conclude that, within these models, a consistent description of direct photons and hadrons is possible. While only more complex and accurate models can give a definitive answer, this already suggests that

a significant direct photon production in a later stage of the system evolution might indeed be the reason for the measured high elliptic flow.

One possible candidate for such a more complex and accurate model would be one including a description of the time evolution of the system. Such a model has been conceived, but could unfortunately not be implemented within the limited time span of this bachelor thesis.

All in all the models developed in this thesis do a very good job at describing the data of various measurements. Although there could not be a definite answer provided to whether or not direct photons arise to a substantial amount during a later stage of the evolution of the collision system, there are clear indications that point to this scenario. The already conceived time evolution model could bring further clarity to this question.

Bibliography

- [1] DESY. Das Standardmodell der Teilchenphysik. http://www.weltmaschine.de/physik/standardmodell_der_teilchenphysik/, 2013. online; accessed 2013-07-09.
- [2] CERN. The Large Hadron Collider. <http://home.web.cern.ch/about/accelerators/large-hadron-collider>, 2013. online; accessed 2013-07-09.
- [3] CERN. The Search for the Higgs boson. <http://home.web.cern.ch/about/physics/search-higgs-boson>, 2013. online; accessed 2013-07-09.
- [4] CERN. ALICE. <http://home.web.cern.ch/about/experiments/alice>, 2013. online; accessed 2013-07-09.
- [5] Daniel Lohner for the ALICE Collaboration. Measurement of Direct-Photon Elliptic Flow in Pb-Pb Collisions at $\sqrt{s_{NN}} = 2.76$ TeV. 2012.
- [6] Paul Stankus. Direct Photon Production in Relativistic Heavy-Ion Collisions. *Annual Review of Nuclear and Particle Science*, 55(1):517–554, 2005.
- [7] The ROOT Team. What is ROOT? <http://root.cern.ch/drupal/content/about>, 2013. online; accessed 2013-07-05.
- [8] Kohsuke Yagi, Tetsuo Hatsuda, and Yasao Miake. *Quark-Gluon Plasma: From Big Bang to Little Bang*. Cambridge University Press, 2005.
- [9] Ramona Vogt. *Ultrarelativistic Heavy-Ion Collisions*. Elsevier, 2007.
- [10] Wojciech Florkowski. *Phenomenology of Ultra-Relativistic Heavy-Ion Collisions*. World Scientific Publishing Co. Pte. Ltd., 2010.

- [11] P.J. Mohr, B.N. Taylor, and D.B. Newell. The 2010 CODATA Recommended Values of the Fundamental Physical Constants (Web Version 6.0). 2011. online; accessed 2013-06-17.
- [12] Cheuk-Yin Wong. *Introduction to High-Energy Heavy-Ion Collisions*. World Scientific Publishing Co. Pte. Ltd., 1994.
- [13] Miklos Gyulassy. The QGP Discovered at RHIC. 2004.
- [14] Eric Hand on the Nature News Blog. Hot Stuff: CERN physicists create record-breaking subatomic soup. <http://blogs.nature.com/news/2012/08/hot-stuff-cern-physicists-create-record-breaking-subatomic-soup.html>, August 2012. online; accessed 2013-07-09.
- [15] Y. Aoki, Sz. Borsanyi, S. Durr, Z. Fodor, S. D. Katz, S. Krieg, and K. K. Szabo. The QCD transition temperature: results with physical masses in the continuum limit II. 2009.
- [16] Owe Philipsen. The QCD equation of state from the lattice. 2012.
- [17] ALICE Collaboration. Centrality dependence of π , K, p production in Pb-Pb collisions at $\sqrt{s_{NN}} = 2.76$ TeV. 2013.
- [18] Klaus Reygers. private communication.
- [19] Matthew Luzum. Flow fluctuations and long-range correlations: elliptic flow and beyond. 2011.
- [20] F. James and M. Roos. Minuit: A System for Function Minimization and Analysis of the Parameter Errors and Correlations. *Comput.Phys.Commun.*, 10:343–367, 1975.
- [21] ALICE Collaboration. Pion, Kaon, and Proton Production in Central Pb-Pb Collisions at $\sqrt{s_{NN}} = 2.76$ TeV. 2012.
- [22] Martin Wilde for the ALICE Collaboration. Measurement of Direct Photons in pp and Pb-Pb Collisions with ALICE. 2012.
- [23] Werner Vogelsang. private communication.

Bibliography

- [24] PHENIX Collaboration. Enhanced production of direct photons in Au + Au collisions at $\sqrt{s_{\text{NN}}} = 200$ GeV and implications for the initial temperature. December 22 2009.
- [25] PHENIX Collaboration. Observation of direct-photon collective flow in Au+Au collisions at $\sqrt{s_{\text{NN}}} = 200$ GeV. August 22 2011.
- [26] WA98 Collaboration. Direct Photon Production in 158 A GeV 208Pb + 208Pb Collisions. June 13 2000.
- [27] WA98 Collaboration. Interferometry of Direct Photons in Central 280Pb+208Pb Collisions at 158A GeV. 2003.
- [28] Hannu Holopainen, Sami Räsänen, and Kari J. Eskola. Elliptic flow of thermal photons in heavy-ion collisions at Relativistic Heavy Ion Collider and Large Hadron Collider. 2011.
- [29] Hannu Holopainen and Sami Räsänen, 2012. private communication.
- [30] Marian Ivanov for the ALICE Collaboration. Identified charged hadron production measured with ALICE at the LHC. 2013.
- [31] Francesco Noferini for the ALICE Collaboration. Anisotropic flow of identified particles in Pb-Pb collisions at $\sqrt{s_{\text{NN}}} = 2.76$ TeV measured with ALICE at the LHC. 2012.
- [32] J. Beringer et al. Review of Particle Physics. *Phys. Rev. D*, 86:010001, Jul 2012.
- [33] David d'Enterria and Dmitri Peressounko. Probing the QCD equation of state with thermal photons in nucleus-nucleus collisions at RHIC. 2005.

Acknowledgements

First of all I would like to thank Priv.-Doz. Klaus Reygers for his great instructions and making this thesis possible in the first place. I would similarly like to thank Prof. Dr. Norbert Herrmann for his willingness to act as second examiner.

Special thanks go to Werner Vogelsang, Hanno Holopainen, and Sami Räsänen, who provided me with the results of their calculations.

I also express my sincere gratitude to Mr. Daniel Lohner for his helpful advice, help when it was most needed, and vital input in many situations as well as for proofreading this thesis. In addition, I thank all the other members of the ALICE group at the Physikalisches Institut for their invaluable input and help with smaller and bigger problems.

Furthermore, my thanks go to my fellow occupants of the cool bachelor students' room for making the time while writing this thesis not dull and always providing topics to talk about. In addition, I want to thank the members of the IT team of the Physikalisches Institut for fixing the occasional software issue promptly and expertly, thus enabling a steady workflow.

I also thank my Chinese teacher, Mr. Song, not only for making the Chinese language easy to pick up and its words manageable to pronounce, but also for not making me explain my research in Chinese. Besides, my thanks go to my various sparring partners in the Ju-Jutsu classes, who helped me to fight better and left my hands intact enough to operate a keyboard on the following day.

Then, I would like to thank my parents for their ongoing affectionate backing and support for my studies and my life. Last but not least, I also owe a great amount of gratitude to my brother, who not only always has great advice and funny stories, but also helped me to improve my phrasing and wording in this thesis.

Erklärung/Declaration

Ich versichere, dass ich diese Arbeit selbstständig verfasst und keine anderen als die angegebenen Quellen und Hilfsmittel benutzt habe.

Heidelberg, den

I hereby confirm that the thesis is my own work; and that all published or other sources of material consulted have been acknowledged in notes to the text or the bibliography.

Heidelberg,

(Tobias Denz)